Available online at www.sciencedirect.com

ScienceDirect

Geochimica et Cosmochimica Acta 124 (2014) 170–189

Geochimica et Cosmochimica Acta

www.elsevier.com/locate/gca

Gas chemistry, boiling and phase segregation in a geothermal system, Hellisheidi, Iceland

Samuel Scott [a,c,*], Ingvi Gunnarsson [b], Stefán Arnórsson [c], Andri Stefánsson [c]

[a] *Reykjavik Energy Graduate School of Sustainable Systems, Reykjavik Energy, Baejarhals 1, 110 Reykjavik, Iceland*
[b] *Reykjavik Energy, Baejarhals 1, 110 Reykjavik, Iceland*
[c] *Institute of Earth Sciences, University of Iceland, Sturlugata 7, 101 Reykjavik, Iceland*

Received 22 March 2013; accepted in revised form 19 September 2013; Available online 3 October 2013

Abstract

The geochemistry of aquifer fluids of the Hellisheidi geothermal system, southwest Iceland, was studied. Based on samples of vapor and liquid from well discharge fluids, the aquifer fluid compositions at the depth of the geothermal system were reconstructed taking into account the highly variable degree of excess well discharge enthalpy, where the enthalpy of the discharge is significantly higher than that of vapor-saturated liquid at the measured aquifer temperature. Decreasing concentrations of non-volatile components such as Si in the total well discharge suggest that the main cause of elevated discharge enthalpies is liquid–vapor phase segregation, i.e. the retention of liquid in the aquifer rock due to its adhesion onto mineral surfaces. Moreover, the slightly lower than equilibrium calculated concentrations of H_2 and H_2S in some of the hottest and highest-enthalpy wells is considered to be caused by conductive heat transfer from the rocks to the fluids. Alternatively, the cause may lie in the selection of the phase segregation conditions. The calculated concentrations of volatile species in the aquifer fluid are very sensitive to the assumed phase segregation conditions while non-volatiles are not greatly affected by this model parameter. In general, the level of uncertainty does not contradict previous findings of a close approach to fluid–mineral equilibrium at aquifer temperatures above 250 °C. The CO_2 concentrations were observed to fall below equilibrium with respect to the most likely mineral buffers, suggesting a possible source control. Elevated H_2 concentrations indicate a small equilibrium vapor fraction in aquifer fluids (~0.2% by mass or ~3% by volume). Previous conceptual models of the Hengill volcanic area (e.g. Bödvarsson et al., 1990) have implied a central magmatic heat source underlying the Hengill central volcano. Instead, a new conceptual model of the Hellisheidi system is proposed that features two main regions of fluid upflow heated by a complex of dikes and sills associated with an eruptive fissure active during the Holocene.

1. INTRODUCTION

The state of knowledge of volcanic geothermal systems has been greatly advanced in recent decades by studying fluids and mineralogy from wells drilled deep into the systems. These studies have revealed that secondary mineral–fluid equilibria is closely approached in such systems for most components, at least when temperatures exceed ~150 °C (Browne and Ellis, 1970; Browne, 1978; Ellis and Mahon, 1977; Giggenbach, 1980, 1981, 1988; Arnórsson et al., 1983; Stefánsson and Arnórsson, 2000, 2002). The concentrations of non-volatiles such as chlorine and volatiles like carbon and sulfur may also be source controlled, originating from recharging waters, magmatic gas, and rock dissolution (Ármansson et al., 1982; Giggenbach, 1992). However, one major problem in reconstructing aquifer fluid compositions from measurements of the liquid and vapor discharged at the surface is that wells drilled into boiling,

* Corresponding author. Present address: Institute of Geochemistry and Petrology, ETH Zürich, Clausiusstrasse 25, 8092 Zürich, Switzerland. Tel.: +41 78 606 97 75.
E-mail address: samuel.scott@erdw.ethz.ch (S. Scott).

0016-7037/$ - see front matter © 2013 Elsevier Ltd. All rights reserved.
http://dx.doi.org/10.1016/j.gca.2013.09.027

high-enthalpy systems often show 'excess' enthalpy, or a higher vapor-to-liquid ratio, than result from adiabatic boiling of a vapor-saturated liquid at the measured aquifer temperatures (Pruess and Narasimhan, 1982, D'Amore and Celati, 1983; D'Amore and Truesdell, 1985; Arnórsson et al., 1990, 2010; Karingithi et al., 2010; Stefánsson et al., 2011). As a result, quantitative understanding of fluid sources, mass movement and processes occurring in the geothermal aquifers and acting upon fluid ascent to the surface is often difficult.

Depressurization boiling along water vapor saturation in producing aquifers and wells of volcanic geothermal systems causes cooling and elemental separation between vapor and liquid produced. Volatiles such as CO_2, H_2S and H_2 preferentially enter the vapor phase whereas non-volatiles including Si, Na and Cl become enriched in the boiled liquid. This may lead to physiochemical changes of the system including mineral supersaturation and precipitation, thus changing the composition of the aquifer fluid upon ascent to the surface where samples are commonly collected at the wellhead. Heat transfer from the hot rock to the rising fluid may enhance boiling, resulting in an increased vapor fraction or enthalpy at the surface without affecting the total (two-phase) chemical composition. Previous studies have shown that adhesion of the liquid phase onto mineral surfaces in the porous, fractured aquifer rock upon rapid depressurization boiling, termed 'phase segregation', is dominantly responsible for producing excess well discharge enthalpies in boiling geothermal systems (Arnórsson et al., 1990, 2010; Gudmundsson and Arnórsson, 2002; Karingithi et al., 2010). Physically, this process is a consequence of the low relative permeability of liquid and high capillary pressures that develop at intermediate vapor saturations. For wells affected by phase segregation, models aimed at reconstructing initial aquifer fluid chemical compositions from surface discharge measurements need to take into account open-system boiling processes.

This study extends the work of Arnórsson et al. (1990, 2007, 2010) aimed at quantitative modeling of aquifer fluids in geothermal systems from samples collected at the surface. In previous studies, the level of uncertainty associated with the model calculations was unclear. This study seeks to constrain this uncertainty, especially for volatile components, both by theoretical consideration of the equations of mass and energy conservation and direct application by calculating aquifer fluid compositions for a multitude of excess enthalpy discharge samples at a wide range of possible phase segregation conditions. Moreover, the dataset was used to construct a conceptual geochemical model of the reservoir that describes the fluid upflow and recharge zones. More generally, this study highlights the challenges posed by boiling geothermal systems in terms of assessing aquifer fluid geochemistry for excess enthalpy well discharges observed in a wide variety of settings (e.g. Arellano et al., 2005). Additionally, it demonstrates that, despite the uncertainties resulting from chemical analysis and model calculations, fluid geochemistry can provide a coherent picture of the physiochemical state of high-temperature geothermal reservoirs.

2. THE HELLISHEIDI GEOTHERMAL SYSTEM

The Hellisheidi geothermal system, located in SW-Iceland, is a part of the Hengill volcanic system, situated at the juncture of the North American plate, the Eurasian plate and the Hreppar microplate (Fig. 1). The two largest geothermal power plants in Iceland are being operated in the area, Nesjavellir (120 MWe installed electrical capacity + 300 MWth thermal energy) and Hellisheidi (303 MWe + 133 MWth). The dominant structure is a SW–NE oriented complex of normal faults and volcanic fissures that has produced thick sequences of basaltic hyaloclastites and lava flows (Sæmundsson, 1967, 1992). Postglacial volcanism at Hengill has been confined to three major events dated at ~10,300, ~5700 and ~1800 years b.p., respectively (Sinton et al., 2005). The heat source for the system is believed to be a complex of solidified dykes, sills and intrusions that are scarce above 1.5 km depth but become dominant with increasing depth (Árnason et al., 2010).

The primary rocks associated with the Hengill system are mostly basaltic with layers of subglacially erupted hyaloclastic formations intercalated with subaerially erupted lava flows. The primary mineralogy of the rocks consists of olivine and plagioclase phenocrysts with plagioclase, pyroxene, olivine, Ti–Fe oxides and glass in the groundmass (Sæmundsson, 1967, 1992). Subsurface alteration mineralogy in the Hellisheidi system consists of four alteration zones with increasing depth (temperature): the smectite–zeolite zone, the mixed-layer clay zone, chlorite–epidote zone and the epidote–actinolite zone. Other common alteration minerals include quartz, calcite, prehnite, Fe-sulfides, K-feldspar and albite, wollastonite and wairakite (>180 °C) (Schiffman and Fridleifsson, 1991; Larsson et al., 2002). Episodes of heating or cooling may cause secondary minerals to be present that do not match the existing reservoir temperature.

Previous conceptual models of the Hengill area have invoked a common upflow zone for the two wellfields linked to a shallow magma chamber located underneath the Hengill central volcano (Bödvarsson et al., 1990). However, direct temperature measurements obtained from recent deep drilling in the northern part of the Hellisheidi well-field show decreasing temperatures toward the Hengill central volcano (Gunnarsson et al., 2010). The reduction in seismic wave velocities observed >3 km depth is stronger for *P*- than *S*-waves, contrary to what would be expected if a shallow magma chamber were present (Foulger, 1995; Tryggvason et al., 2002). Additionally, the ∂D values of Nesjavellir discharge fluids are close to that of present-day precipitation found in the southern part of the Langjokull icecap 60–80 km to the northeast (−72‰ to −77‰) (Sveinbjörnsdottir and Johnsen, 1992), while the ∂D values of well discharges in the Hellisheidi area are much higher (~−65‰), closer to the values observed in local precipitation (Mutonga et al., 2010). This evidence suggests that the Nesjavellir and Hellisheidi wellfields have distinct fluid source regions, and by implication, do not share a common upflow zone.

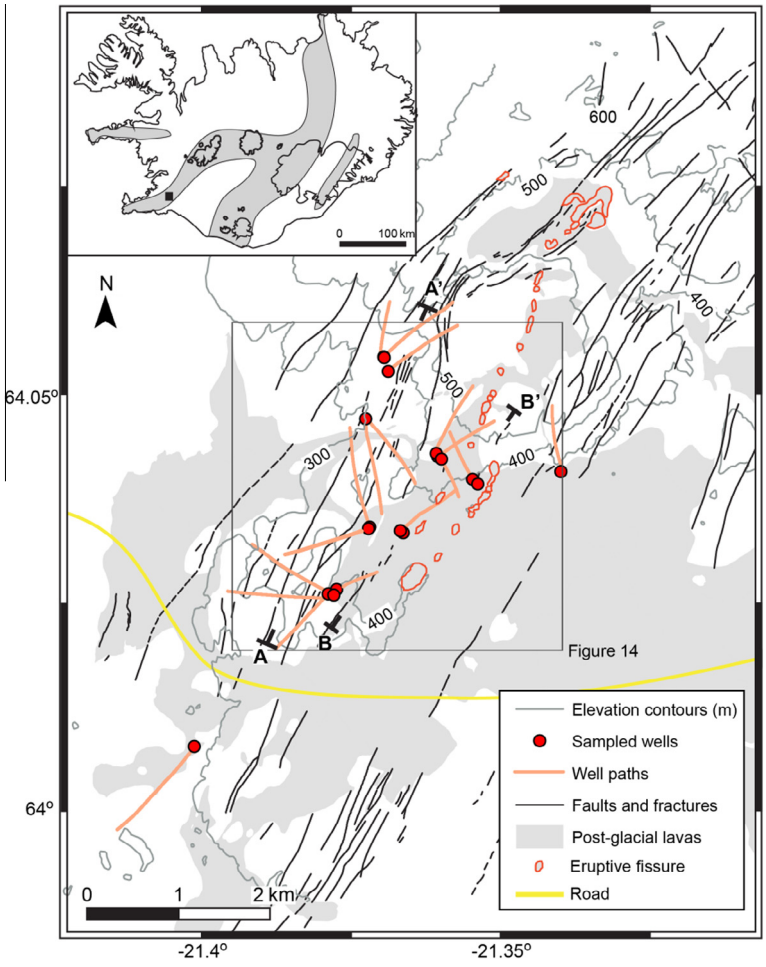

Fig. 1. Map of the Hellisheidi geothermal area. Inset shows the approximate locations of the main active volcanic belts and the location of the study area in SW-Iceland.

3. SAMPLING AND ANALYSIS

The basis of this study is 33 two-phase well discharge samples collected in 2008–2010. The sampling and analytical procedures have been previously described in detail (Arnórsson et al., 2006). A summary of the analytical methods and precision is provided in Table 1. The analytical uncertainties indicated by Table 1 and the ionic balance for each sample listed in Table 2 are generally smaller than the uncertainties related to model calculations of aquifer fluid compositions, as discussed in detail below.

The liquid and vapor phases were separated using a Webre separator. Vapor samples were collected into evacuated gas bulbs containing 5–10 ml 50% w/v KOH. The concentrations of CO_2 and H_2S in the vapor condensate were determined by modified alkalinity titration (Stefánsson et al., 2007) and a precipitation titration method using Hg-acetate and dithizone indicator (Arnórsson et al., 2006), respectively. The non-condensable gases including H_2, N_2, Ar and CH_4 were analyzed by gas chromatography (GC).

The liquid phase samples were cooled down using a stainless steel spiral that was connected to the Webre separator and filtered through 0.2 μm filters (cellulose acetate) into polypropylene and amber glass bottles. Samples for major cation analysis were acidified with 0.5 ml concentrated HNO_3 (Suprapur, Merck) per 100 ml sample and determined using ICP-OES. Two samples for major anion analysis were collected, one not further treated for F and Cl determination and another to which 2% Zn-acetate solution was added for SO_4 analysis. All anion analyses were carried out using ion chromatography (IC). Samples for determination of CO_2 were collected into amber glass bottles and analyzed using the modified alkalinity titration previously mentioned (Stefánsson et al., 2007). Dissolved H_2S was titrated on-site using the method previously described (Arnórsson et al., 2006). The pH was analyzed on-site and in-line within a few seconds of sampling at ~20 °C using a flow-through cell.

4. LIQUID AND VAPOR COMPOSITION

The chemical compositions of the liquid and vapor samples collected at Hellisheidi are listed in Table 2. The fluids are dilute (<500 ppm Cl) and typical for systems recharged by meteoric water in Iceland (Arnórsson, 1995). The

Table 1
Summary of analytical methods used for liquid and vapor phase samples and precision obtained for duplicate (liquid phase) or replicate (vapor phase) analyses.

Component	Analytical method	Measured concentration range (ppm)	Mean % deviation[a]	Standard deviation[b]
Liquid phase				
CO_2	Titration	9.96–87.8	4.8	3.4
H_2S	On-site titration	22.9–75.1	1.0	0.7
Si	ICP-OES	626–1012	0.5	0.3
B	ICP-OES	0.38–2.52	0.9	0.5
Na	ICP-OES	137.9–256.9	0.9	0.6
K	ICP-OES	25.5–47.8	0.6	0.3
Ca	ICP-OES	0.22–1.29	2.4	1.9
Mg	ICP-OES	<0.001–0.0065	16.7	11.2
Fe	ICP-OES	<0.005–0.072	4.4	2.9
Al	ICP-OES	1.19–2.01	0.5	0.4
Cl	IC	101.3–205.0	0.5	0.2
SO_4	IC	6.3–19.1	0.9	0.5
F	IC	0.5–1.4	2.7	1.4
Vapor phase				
CO_2	Titration	1191–7259	4.1	1.6
H_2S	Titration	190–1183	4.6	2.4
H_2	GC	0.6–68.7	3.8	2.3
CH_4	GC	0.6–15.2	4.7	2.9
N_2	GC	14.6–577	10.6	6.2
Ar	GC	0.38–19.39	17.4	9.1

[a] Mean percentage difference between duplicate/replicate determinations.
[b] Standard deviation of mean percentage deviation.

measured discharge enthalpies ranged from 1043 to 2757 kJ kg^{-1}. Of the 21 wells sampled only four are liquid enthalpy, where the enthalpy of the produced fluid is the same within the error of measurement as that of steam-saturated liquid at the aquifer temperature (i.e. $h^{d,t} = h^{f,l}$). The other wells display variable degrees of excess enthalpy, with three of the wells discharging almost dry steam.

Silica, Na and Cl are the dominant components in the liquid phase with concentrations in the range of 613–1010 ppm, 22.6–255 ppm and 25.7–362 ppm, respectively. The volatile gases including CO_2 and H_2S are preferentially found in the vapor phase at the sampling pressures (4–15 bar) with concentrations in the range 758–7587 ppm and 119–1607 ppm, respectively. Nonetheless, considerable concentrations are also dissolved in the sampled liquid phase, with up to 93.3 and 77.4 ppm CO_2 and H_2S, respectively. The other major gases include H_2, N_2, Ar and CH_4 with concentrations in the vapor of 0.6–68.5 ppm, 14.7–577 ppm, 0.4–22.2 ppm and 0.6–15.2 ppm, respectively.

5. PROCESSES LEADING TO EXCESS ENTHALPY

Aquifers of liquid dominated high-temperature geothermal systems may be either sub-boiling or consist of two phases, liquid and vapor. In the case of sub-boiling aquifers, pressure drop due to decreased hydrostatic head of the ascending fluid results in boiling within the well. Under these conditions, it is reasonable to assume that the system is isolated, i.e. the enthalpy and the mass of the aquifer fluid are conserved on the way up to the surface. Such well discharges are characterized by low to intermediate discharge enthalpy (>1200 kJ kg^{-1}) depending on the aquifer temperature (usually >275 °C). In the case of two-phase aquifers, intensive boiling begins in the aquifer rock itself upon depressurization or addition of heat. Well discharge enthalpies from such systems can be greatly in excess of the initial fluid enthalpy, even approaching that of pure vapor (~2780 kJ kg^{-1}). Depressurization is accompanied by a decrease in fluid temperature along the two-phase saturation curve, resulting in the establishment of a temperature gradient between rock and fluid initially in thermal equilibrium (Henley and Hughes, 2000). Conductive heat transfer from the aquifer rock to the fluid increases the relative proportion of steam without affecting the total two-phase fluid composition. It is likely to be most significant where a decrease in fluid pressures has led to the development of extensive boiling zones within the rock formation, as the maximum heat gain from conductive heat transfer from the rock formation to the fluid flowing up the wellbore is likely to be only on the order of 0.1 MW (Grant and Bixley, 2011).

Consideration of the flow and physical properties of liquid/vapor and geochemical evidence indicate that segregation of liquid and vapor during flow toward the wellbore is the dominant cause of excess discharge enthalpies. Due to the much lower density of vapor, the liquid rapidly becomes volumetrically a relatively minor component of the flow upon depressurization boiling (i.e. for a fluid at the boiling point with $S^l = 1$ at $T^f = 300$ °C that cools to 275 °C, $S^l \sim 0.3$). The strong decrease in the relative permeability of liquid at intermediate vapor saturations and high capillary pressures contribute to causing liquid to

Table 2
Chemical composition of geothermal well discharges collected at Hellisheidi, SW Iceland.

Sample #	Well #	$h^{d,t}$, kJ kg^{-1}	p^{s}, bar-g	p^{wh}, bar-g	T^{f}_{qtz}, °C	$T^{f}_{Na/K}$, °C	Liquid phase (ppm)														Ionic balance (% diff.)[a]	Vapor phase (ppm)					
							pH / °C	SiO_2	B	Na	K	Mg	Ca	Al	Fe	F	Cl	CO_2	H_2S	SO_4		CO_2	H_2S	H_2	CH_4	N_2	Ar
10-5079	HE-47	2139	11	24	323	301	8.14 / 21	1010	1.80	148	36.3	0.001	0.27	1.58	0.008	1.07	203	46.7	22.9	6.4	−3.4	2281	767	28.5	1.93	21.6	0.64
10-5080	HE-19	1599	10.7	20.2	266	247	8.80 / 23	632	1.20	196	31.2	0.001	0.58	1.53	0.015	1.06	187	10.0	66.8	8.2	4.9	2306	871	32.0	2.12	16.1	0.56
10-5081	HE-30	2173	9.6	16.1	315	286	8.25 / 22	974	1.45	164	36.0	0.001	0.34	1.60	0.009	1.06	203	22.1	35.0	9.7	1.3	3736	865	28.3	2.82	21.0	0.63
10-5082	HE-15	1597	9.8	22.5	274	252	8.79 / 20	684	1.13	182	30.0	0.002	0.49	1.56	0.008	1.07	167	16.4	55.5	9.6	5.5	3660	823	18.7	3.32	55.8	1.24
10-5083	HE-17	2054	9.5	21.8	288	271	8.48 / 23	784	1.48	189	36.6	0.004	0.32	1.71	0.015	1.09	205	13.7	64.5	12	1.8	2938	1229	56.3	3.34	25.8	1.03
10-5084	HE-11	2047	9.6	19	282	268	8.71 / 22	744	1.07	173	32.9	0.002	0.22	2.01	0.007	0.97	161	47.4	52.1	11.9	0.4	4352	737	35.5	3.72	28.4	1.11
10-5085	HE-06	1548	9.6	18.5	264	248	8.67 / 23	628	0.67	162	25.7	0.006	0.49	1.93	0.070	1.02	101	87.8	57.3	9.1	−1.5	7587	723	35.9	3.06	31.6	1.05
10-5086	HE-46	1177	8	16	270	258	9.26 / 22	668	0.39	177	30.8	0.003	0.52	1.96	0.015	1.16	63	29.5	33.3	42.5	13.1	4256	206	0.7	6.93	208.2	6.20
10-5087	HE-52	1169	4	9.6	265	248	9.22 / 27	678	0.48	178	28.5	0.001	1.27	1.87	0.008	1.44	78	20.1	26.4	30.5	12.6	3922	119	2.0	15.22	457.8	22.16
10-5163	HE-18	1385	10.1	13.7	274	257	8.92 / 21	678	0.88	170	29.5	0.001	0.31	1.90	<0.005	0.98	144	34.9	52.0	19.7	1.0	2435	639	25.8	6.58	70.1	1.76
10-5164	HE-09[e]	2757	10.5	13	289	275	7.25 / 186	819	2.67	172	34.6	0.010	1.18	1.20	0.141	0.89	204	29.4	74.7	-	−6.7	2593	1412	57.8	0.99	14.7	0.60
10-5165	HE-57	1043	6.2	12.5	279	266	9.14 / 20	743	1.06	195	36.4	0.001	0.99	1.57	<0.005	0.50	155	46.7	50.9	19.1	1.2	2904	405	2.4	7.65	254.5	8.79
10-5166	HE-03	1216	11.3	12.7	273	266	8.80 / 20	665	1.08	255	47.7	0.000	0.73	1.19	<0.005	0.87	362	10.0	45.3	11.1	−2.2	998	398	2.3	1.99	270.6	6.38
10-5168	HE-12	1746	10.2	19.5	290	268	8.66 / 24	783	1.33	193	36.7	<0.001	0.32	1.90	0.007	0.95	193	22.1	73.4	17.9	−0.2	2504	933	36.9	3.64	25.8	0.76
10-5169	HE-07	1372	10.2	21	267	253	8.89 / 23	636	1.24	198	33.2	<0.001	0.36	1.68	<0.005	1.13	185	16.4	73.6	8.3	1.9	1638	754	26.1	3.02	214.2	3.74
10-5170	HE-45[d]	2498	10	24.5		270			2.51	28	5.40						179					1785	856	27.6	0.58	15.8	0.57
10-5171	HE-42	2489	10.1	24.5	301	284	8.35 / 19	874	2.50	139	30.0	0.001	0.24	1.75	0.022	1.35	169	13.6	35.0	3.1	1.5	758	1030	38.9	1.06	19.4	0.73
10-5172	HE-41[d]	2704	10.2	24.5		285			0.53	22.6	4.9						26					2123	769	30.2	0.69	15.1	0.44
09-5189[b]	HE-43	1466	4.6	16.1	295	272	8.42 / 24	877	1.54	143	28.1	0.002	1.05	2.29	0.010	1.10	90	33.0	50.0	10.6	10.5	3886	965	26.4	4.07	576.9	9.80
09-5190[b]	HE-05	1194	10.8	17	274	262	9.20 / 22	676	0.41	161	29.1	0.001	0.4	1.91	<0.01	1.72	77	66.8	46.0	16.2	1.1	3670	245	0.6	6.79	135.1	2.82
09-5198[b]	HE-06	1548	11.6	16	264	247	8.70 / 23	613	0.69	160	25.4	0.001	0.49	1.87	<0.01	0.70	104	74.8	60.1	11.3	1.4	7173	735	22.0	2.41	26.6	0.56
09-5199[b]	HE-17	2319	12.5	25	292	272	8.37 / 23	786	1.64	190	37.3	0.002	0.35	1.69	<0.01	0.78	216	15.4	68.7	5.6	0.03	2790	1586	51.1	2.47	33.1	0.74
09-5197[b]	HE-29	2399	11	20.5	305	280	8.67 / 22	885	5.63	132	27.6	0.135	0.59	2.35	0.042	1.61	105	18.1	52.1	2.8	1.35	2552	1117	41.0	5.58	215.2	4.14
09-5200[b]	HE-41	2704	12.2	17	291	277	8.70 / 15	710	1.02	72	14.7	0.005	0.17	2.29	0.037	1.05	41	93.3	57.6	2.9	−22.1	1980	723	25.9	0.74	54.9	0.93
08-3001[c]	HE-07	1372	8.5	20	269	250	9.13 / 17	659	1.23	201	32.7	0.012	0.35	1.74	0.011	1.10	199	7.4	76.1	7.5	-0.4	1309	822	26.2	3.96	92.5	2.16
08-3002[c]	HE-12	1746	9.5	17	294	267	8.66 / 19	816	1.36	188	35.5	0.005	0.28	1.90	0.030	1.26	196	11.0	77.4	13.7	0.07	2325	1147	49.8	5.49	281.9	5.83
08-3003[c]	HE-17	2319	10	20.8	289	277	8.47 / 17	796	1.47	177	36.2	0.002	0.27	1.68	0.009	1.00	207	10.6	68.0	5.5	3.6	3161	1607	68.5	4.54	290.0	5.43
08-3004[c]	HE-11	2047	9.5	18	284	268	8.74 / 17	754	1.04	168	31.8	0.001	0.17	2.03	0.024	1.08	158	22.9	55.7	8.6	3.5	4373	952	43.1	5.71	188.9	3.64
08-3005[c]	HE-29	2399	15	20.8	306	275	8.71 / 21	931	5.92	128	25.7	0.002	0.23	2.17	0.005	1.89	104	11.9	57.5	3.9	3.7	2446	930	36.2	2.84	41.5	1.20
08-3006[c]	HE-05	1194	8.8	16.2	276	260	9.42 / 20	698	0.40	157	27.9	0.000	0.32	2.01	0.011	2.08	77	33.1	37.7	19.2	0.7	3558	210	1.2	10.59	248.8	5.91
08-3007[c]	HE-06	1548	9.5	18	265	245	8.82 / 21	633	0.68	160	24.9	0.001	0.37	1.95	0.004	0.91	107	34.5	56.9	10.4	1.5	6831	654	27.9	3.47	46.0	1.16
08-3009[c]	HE-18	1385	9.4	15.2	273	253	8.97 / 19	682	0.84	165	27.6	0.001	0.31	1.93	0.006	1.16	144	18.9	57.9	8.8	2.0	2853	617	24.4	7.15	137.9	2.64

[a] Calculated as % difference = 100 * (Σcations − Σanions)/(Σcations + Σanions).
[b] Stefánsson et al. (2011).
[c] Remoroza (2010).
[d] Dry-steam well. Analyses of Na, K and B, Cl shown for ratio determination.
[e] Dry-steam well. Liquid phase calculated from 2004 sample at new discharge enthalpy and sampling pressure.

adhere to mineral grain surfaces and remain in the aquifer rock (Sorey et al., 1980; Horne et al., 2000; Pritchett, 2005; Li and Horne, 2007). The retention of liquid in the aquifer is indicated by the observation that the total two-phase concentrations of dissolved solid components, such as silica, strongly decrease with increasing discharge enthalpy, approaching zero as the discharge enthalpy approaches that of dry steam (Fig. 2). When reconstructing aquifer fluid composition from surface discharge measurements of such wells, the basic equations of energy and mass balance comprising the model must take into account open system boiling with loss of liquid between the aquifer and wellhead.

Arnórsson et al. (2007, 2010) considered six processes that may be used to model aquifer fluid composition from data on two-phase well discharges. These models solve equations of mass and energy conservation and use enthalpy as the thermodynamic variable (Appendix 1). They are an approximation, since liquid/vapor enthalpies were obtained for pure H_2O fluids and in the case of large-scale phase separation and fluid expansion during adiabatic decompression, entropy rather than enthalpy should be considered as conserved (Kieffer and Delaney, 1979; Lu and Kieffer, 2009). For all models, the aquifer temperature needs to be selected. In model 1, adiabatic boiling is assumed. In model 2, closed system boiling (conductive heat flow) is assumed. However, in models 3–5 open system boiling is assumed with possible transfer of heat and mass. Model 3 assumes no heat transfer from the aquifer rock upon boiling and that liquid water is partially retained in the aquifer and steam segregates. Models 4 and 5 also assume phase segregation and also allow for steam addition, in the case of model 4, or conductive heat transfer for model 5. Model 6 assumes steam (and gas) loss from the fluid flowing into wells. For these models, the pressure/temperature where liquid and/or vapor are removed and/or added must be defined.

Under isolated and closed system conditions, mass flow and component concentrations are conserved (models 1 and 2). On the other hand, considering phase segregation in the aquifer rock (model 3), a given mass of the residual boiled liquid is retained. Fig. 3 illustrates how the relative mass of the initial 'inflowing' aquifer fluid to the discharge mass flow depends on the selected phase segregation temperature for variable discharge enthalpy. It shows that mass of liquid retained in the aquifer needed to account for a given discharge enthalpy decreases with a lower assumed phase segregation temperature, but is relatively independent of the phase segregation conditions until they approach those of the aquifer. The reason for this is that since less vapor has been generated by boiling at conditions closer to that of the initial aquifer fluid, a greater mass of vapor to liquid segregation is needed in order to account for a given excess discharge enthalpy. Moreover, the greater the degree of excess enthalpy, the greater the fraction of liquid is retained in the aquifer. The results indicate that considerable amount of liquid may be retained (1–2 times the discharge flow rate) in the aquifer for high excess enthalpy wells (>2500 kJ kg^{-1}).

The effect of the phase segregation conditions on the chemical composition of the liquid and vapor phase at

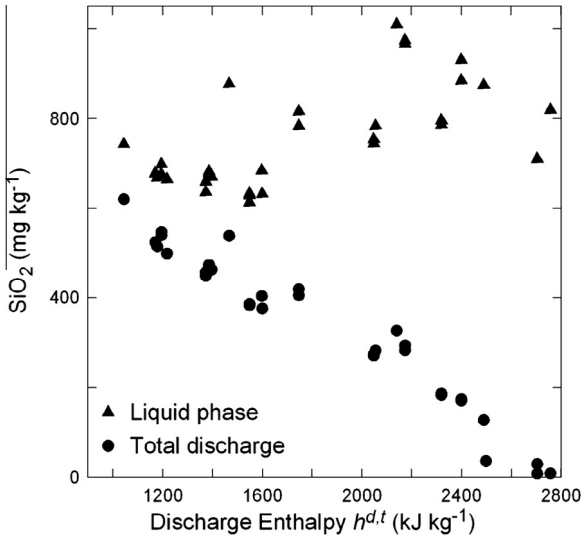

Fig. 2. The concentration of SiO_2 in the liquid phase and total two-phase discharge as a function of discharge enthalpy ($h^{d,t}$).

discharge must be assessed separately for non-volatile and volatile components. For non-volatiles, the discharge concentration of a given component is equal to the initial mass in the aquifer liquid water minus the mass in the retained liquid at the point of phase segregation. For volatiles, the concentration in the discharge fluid is related to the concentration in the initial fluid, the initial and phase segregation temperatures and the distribution coefficient of the volatile component between the two phases. The distribution coefficient is a function of temperature and fluid pressure and is an approximation based on the assumption of equilibrium degassing according to Henry's law and introduces further uncertainty for volatile elements (Appendix 1). An example of the effects of selected phase segregation conditions on the calculated aquifer fluid concentrations of non-volatile and volatile components is shown in Fig. 4 and Fig. 5, respectively. It can be seen from Fig. 4 that the selected phase segregation temperature does not significantly affect the calculated concentrations of non-volatile components in the aquifer fluid except when the phase segregation conditions approach the aquifer conditions and a large fraction of the liquid phase must be retained in the aquifer in order to account for the observed discharge enthalpy. This is in a good agreement with previous findings on the effects of assumed phase segregation conditions on calculated mineral saturation state (Stefánsson and Arnórsson, 2000). On the other hand, the calculated concentrations of volatiles like CO_2, H_2S and H_2 are quite sensitive to the assumed conditions of phase segregation (Fig. 5). The concentrations of volatile elements in the vapor phase rapidly decrease as the vapor fraction rises during boiling; in order to account for the measured discharge concentration, a higher initial aquifer fluid concentration is calculated according to model 3 if lower phase segregation temperatures are assumed. The uncertainty of reconstructed volatile aquifer concentrations is greater in wells with a larger degree of excess enthalpy.

The possible contribution of added vapor (model 4) or conductive heat transfer (model 5) to excess enthalpy

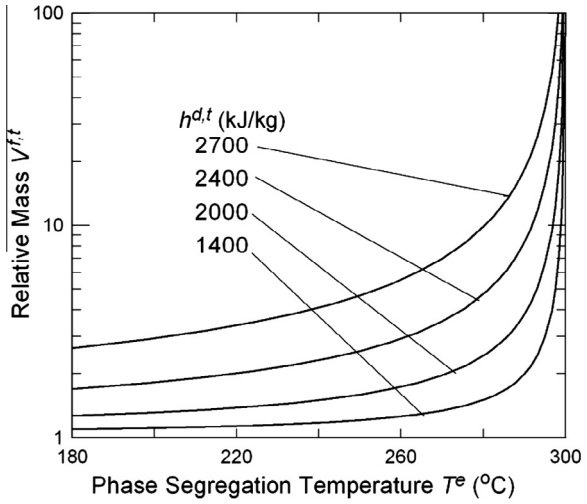

Fig. 3. Calculated relative mass of initial aquifer fluid to the mass of the total discharge ($V^{f,t} = M^{f,t}/M^{d,t} = (h^{d,t} - h^{e,l})/(h^{f,t} - h^{e,l})$) as a function of phase segregation temperature (T^e) for wells having variable discharge enthalpy ($h^{d,t}$). The initial aquifer fluid was assumed to have vapor-saturated liquid enthalpy at temperature (T^f) of 300 °C. For this example, the mid-point phase segregation pressure would correspond to a temperature of 264 °C.

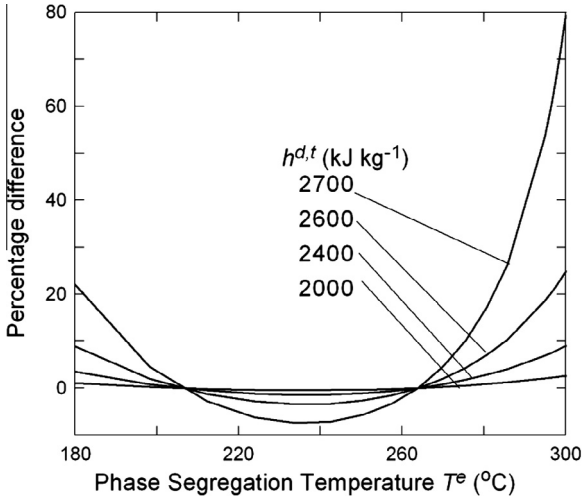

Fig. 4. Percentage difference between the calculated concentration of a non-volatile component in the initial aquifer fluid assuming a given phase segregation temperature (T^e) and the calculated concentration at a reference point (zero difference) using the 'mid-point' phase segregation pressure ($p^{e,mid}$) of 50 bar (i.e. $T^{e,mid} = 264$ °C), for well discharges having variable discharge enthalpy ($h^{d,t}$). Percentage difference calculated as $(100(m_r^{f,t} - m_r^{f,t,mid})/m_r^{f,t,mid})$ for generic, non-reactive non-volatiles according to model 3. The initial aquifer fluid was assumed to have vapor-saturated liquid enthalpy at a temperature (T^f) of 300 °C.

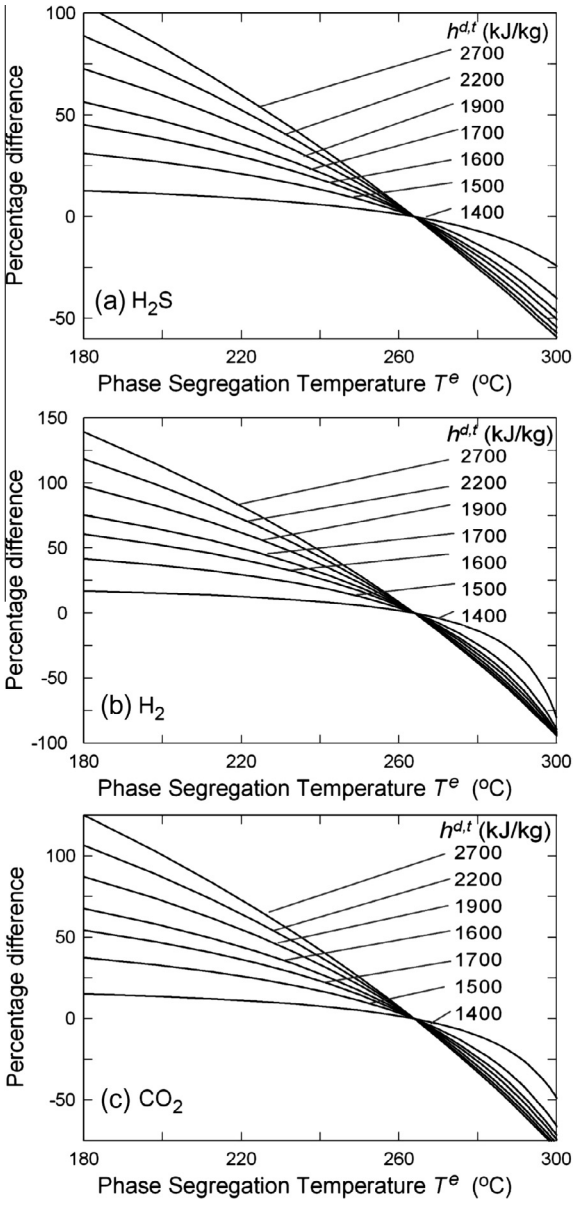

Fig. 5. Percentage difference between the calculated concentration of the volatile components (a) H_2S, (b) H_2, and (c) CO_2, in the initial aquifer fluid assuming a given phase segregation temperature (T^e) and the calculated concentration at a reference point (zero difference) using the 'mid-point' phase segregation pressure ($p^{e,mid}$) of 50 bar (i.e. $T^{e,mid} = 264$ °C), for well discharges having variable discharge enthalpy ($h^{d,t}$). Percentage difference calculated as $(100(m_s^{f,t} - m_s^{f,t,mid})/m_s^{f,t,mid})$. The enthalpy of the initial aquifer fluid was set to vapor-saturated liquid enthalpy at a temperature (T^f) of 300 °C and equilibrium degassing was assumed.

development also increases the uncertainty of calculated component concentrations in the aquifer fluid. Fig. 6 illustrates this by showing how non-volatile and volatile component concentrations could change along the boiling path of an initially liquid-saturated fluid at ~305 °C that develops a discharge enthalpy of ~2400 kJ kg^{-1}. Fig. 6a shows the differences between the different scenarios shown in Fig. 6b and c: while model 3 considers simple phase segregation at ~265 °C, model 4 assumes that 5% of the discharge mass flow resulted from addition of degassed vapor between 265 and 230 °C, model 5a assumes 150 kJ/kg of conductive heat transfer between this same temperature range, and model 5b considers the same amount of

conductive heat transfer but instead prior to phase segregation. Fig. 6b shows that models 4 and 5 result in slightly higher SiO_2 concentrations at discharge compared to model 3; accordingly, reconstructed aquifer fluid compositions assuming model 3 alone could cause one to potentially overestimate the initial aquifer fluid concentration and the temperature derived from quartz geothermometry. In contrast, Fig. 5c shows that possible vapor addition or conductive heat transfer lowers the concentration of a volatile at the point of discharge, especially in the case of model 5b, and assuming model 3 alone would result in a too low calculated volatile concentration in the aquifer fluid.

6. MODELING OF AQUIFER FLUID COMPOSITION, AQUEOUS SPECIATION AND MINERAL SATURATION STATE

In this study, the aquifer fluid compositions were calculated assuming that the excess enthalpy of the well discharges was the consequence of phase segregation alone (model 3). Model 3 was chosen because the calculation procedure can be relatively easily executed using the WATCH program and any assumptions regarding the magnitude of conductive heat transfer (model 5a or b) would be somewhat arbitrary and add further uncertainty to model calculations.

Three parameters must be selected in order to calculate aquifer fluid compositions from wellhead data by the phase segregation model: the temperature and enthalpy of the initial aquifer fluid (T^f, $h^{f,t}$) and the temperature at which phase segregation occurs (T^e). For the present study the aquifer temperature was based on the quartz geothermometer (Gunnarsson and Arnórsson, 2000) except in the case of near dry steam discharges that were calculated using the Na/K geothermometer (Arnórsson and Stefánsson, 1999). These temperatures are listed in Table 2, and it can be seen that Na/K temperatures are systematically 15–20 °C lower than quartz temperatures, as seen in previous studies (Fournier, 1981). This discrepancy could be due to error in the thermodynamic data used for the calculations or non-end member activity of both the Na- and K-feldspars, as compositional data from Nesjavellir has shown secondary Na-feldspar can have a large compositional variation (Larsson et al., 2002). To account for this discrepancy, 15 °C was added to the Na/K temperatures of the dry-steam discharges. This approximation makes the aquifer fluid temperatures of the high-excess enthalpy wells less reliable and potentially a large source of error in the calculated aquifer fluid compositions. The aquifer fluid enthalpy was selected to be that of vapor-saturated liquid at the aquifer temperature ($h^{f,t} = h^{f,l}$).

Selection of the phase segregation temperature or pressure is less straightforward, as phase segregation likely occurs over a temperature or pressure interval rather than at a single point. Although this study assesses the effect of assumed phase segregation conditions by varying this parameter between the extreme possible limits, selection of a 'mid-point' phase segregation pressure $p^{e,mid}$ (corresponding to a vapor saturation temperature $T^{e,mid}$) approximately halfway between the initial aquifer fluid pressure and the wellhead pressure is considered reasonable. This is because the calculated liquid saturation at this temperature based on adiabatic boiling of vapor-saturated liquid

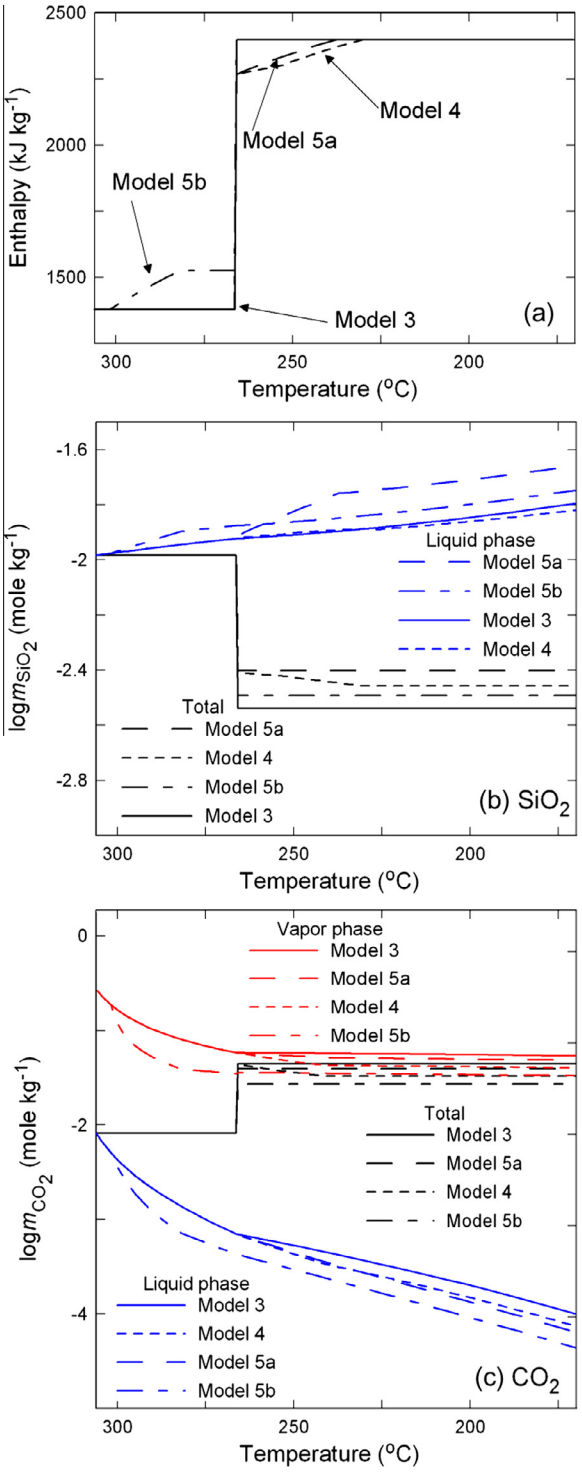

Fig. 6. The (a) total fluid enthalpy, (b) concentration of SiO_2 in the liquid phase and total discharge, and (c) activity of CO_2 in the liquid phase and component concentrations in the vapor phase and total discharge along a boiling path involving phase segregation for a representative 'excess' enthalpy well discharge. See text for differences between the model scenarios shown.

at the inferred aquifer temperature corresponds fairly well to a residual liquid saturation of 0.15–0.3 (Fig. 7), at which point the liquid phase can be expected to become immobile and thus retained in the aquifer (e.g. Piquemal, 1994). The calculations were performed using the WATCH program (Arnórsson et al., 1982; Bjarnason, 2010). A schematic diagram of the calculation procedure is shown in Fig. 8. For liquid enthalpy well discharges, the calculations were carried out in one step whereas for excess enthalpy well discharges, the calculations involved two steps. In step I, component concentrations and speciation were calculated at the point of phase segregation (T^e, p^e) using the measured discharge enthalpy. In step II the computed composition from step I was used to calculate the composition at the aquifer temperature and enthalpy (T^f, h^f). The conditions can either be selected as vapor-saturated liquid enthalpy at T^f or as a higher enthalpy that accounts for the presence of vapor in the aquifer fluid. The possible effects of reactive transport (gain or loss of chemical components) were ignored from model calculations.

While it is often assumed that the enthalpy of the initial aquifer fluid in boiling geothermal systems is that of vapor-saturated liquid at the initial aquifer fluid temperature, in reservoirs where temperatures follow the boiling point curve with depth, some vapor may be present in the initial aquifer fluid. Assuming H_2 or H_2S concentrations in the initial aquifer fluid to be buffered by mineral–gas equilibria, it is possible to use these two gases together to estimate the initial vapor fraction in the aquifer fluid without selecting a phase segregation temperature (Arnórsson et al., 2007) or calculate an equilibrium vapor fraction for each gas separately from individual gas concentrations assuming a selected phase segregation temperature (Appendix 2). Due to the lower solubility of H_2 in liquid water compared to H_2S, H_2 is more sensitive to the presence of a vapor phase than H_2S, and is thus considered a more reliable indicator of the vapor fraction. Sensitivity analyses reveal that the calculated equilibrium vapor fraction is sensitive to both the assumed phase segregation temperature and the selected

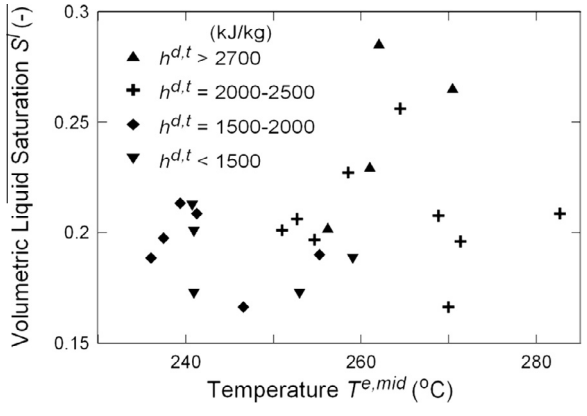

Fig. 7. Calculated liquid volumetric saturation S^l at the temperature corresponding to the 'mid-point' phase segregation pressure $T^{e,mid}$ for the excess enthalpy well discharges considered in this study. Liquid saturation calculated as $S^l = \rho^v(h^{e,v} - h^{f,l})/(h^{f,l}(\rho - \rho^v) - (h^{e,l}\rho^l - h^{e,v}\rho^v))$ (Faust and Mercer, 1979).

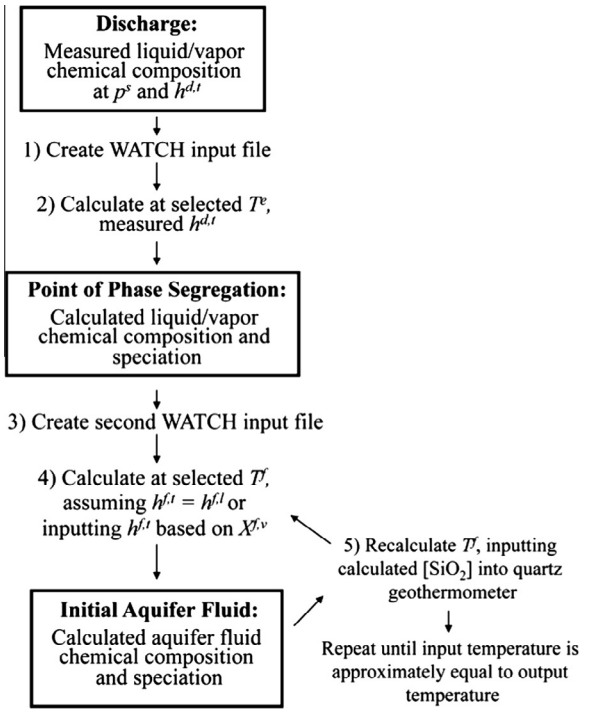

Fig. 8. A schematic diagram of the procedure used to calculate aquifer fluid compositions for excess enthalpy well discharges using the phase segregation model (Appendix A, model 3). The calculations were carried out with the aid of the WATCH program (Arnórsson et al., 1982; Bjarnason, 2010).

reference temperature (Fig. 9). Therefore, reported values should be considered order of magnitude indicators, rather than absolute. Since calculated equilibrium vapor fractions are generally low (<0.5% by mass), non-volatile concentrations in the total aquifer fluid are not significantly affected if

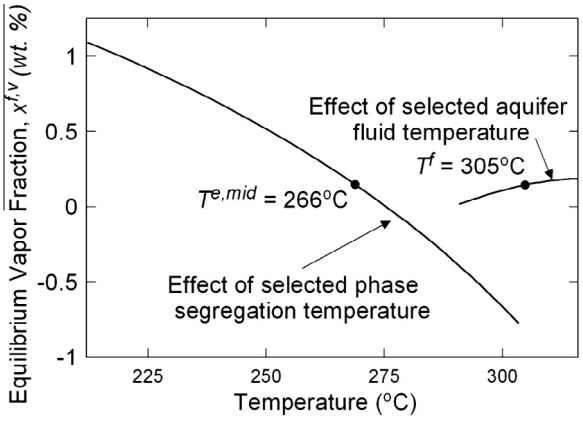

Fig. 9. The sensitivity of calculated equilibrium vapor fraction $x^{f,v}$ to selected phase segregation temperature and initial aquifer fluid temperature, assuming equilibrium of H_2 with respect to the pyrite, pyrrhotite, prehnite and epidote mineral buffer. For this example, $x^{f,v} = 0.2$ if the mid-point phase segregation pressure and temperature according to the quartz geothermometer of Gunnarsson and Arnórsson (2000) is assumed.

the enthalpy of the initial aquifer fluid is adjusted to include the equilibrium vapor fraction.

The aqueous species distribution and mineral saturation states were calculated using the aquifer fluid composition obtained as described above. The thermodynamic database for the speciation calculations is that of Arnórsson et al. (1982) with modifications to gas solubility (Robie and Hemingway, 1995; Fernandez-Prini et al., 2003) and aqueous Al-, Si-, Fe- and carbonate complex stabilities (Plummer and Busenberg, 1982; Pokrovskii et al., 1998; Arnórsson and Andrésdottir, 1999; Arnórsson et al., 2002. The standard thermodynamic properties of minerals used in calculation of equilibrium constants are from Holland and Powell (1998), with the exception of pyrite and pyrrhotite which are from Robie and Hemingway (1995). The standard properties of aqueous species are derived from a variety of sources (Johnson et al., 1992; Pokrovskii and Helgeson, 1995; Robie and Hemingway, 1995; Diakonov et al., 1999; Gunnarsson and Arnórsson, 2000; Fernandez-Prini et al., 2003). The mineral reactions and the respective equilibrium constants together with the source of the data can be found in Karingithi et al. (2010).

7. FLUID–MINERAL EQUILIBRIA

Fluid–rock interaction involves the irreversible dissolution of primary rock-forming minerals to form more stable secondary minerals that can be either thermodynamically stable or metastable under geothermal conditions. Geothermal fluids closely approach saturation with respect to the common secondary geothermal minerals observed under various temperature conditions (Giggenbach, 1980, 1981, 1988; Arnórsson et al., 1983; Stefánsson and Arnórsson, 2000, 2002; Gudmundsson and Arnórsson, 2005; Karingithi et al., 2010). These conclusions are largely based on reconstruction of aquifer fluid composition from data on surface well fluid discharges.

The effect of the phase segregation model parameters on the calculated mineral saturation states in aquifer fluids was systematically investigated in the present study by comparing the results for low-, medium- and high-enthalpy well discharges as well as the selected phase segregation conditions. For each discharge, the selected phase segregation conditions ranged from immediately below the initial aquifer temperature to immediately above the wellhead pressure. An example is given in Fig. 10 for the $Ca^{2+}/(H^+)^2$ activity ratio. Most of the modeled initial aquifer fluid compositions are at near-equilibrium conditions with respect to a mineral assemblage consisting of prehnite, clinozoisite and quartz, especially if a Fe-rich epidote in the pistacite–clinozoisite solid solution is assumed. Although the effect of selected phase segregation conditions on calculated non-volatile concentrations is generally low (Fig. 4) and also depends on reaction stoichiometry, a maximum of approximately 1 log unit of variability in calculated saturated state can result from changing the selected phase segregation temperature between the extreme possible limits. This is mostly due to the effect of segregation conditions on the calculated pH of aquifer fluids, which in turn (at a given temperature) depends on the calculated aquifer fluid

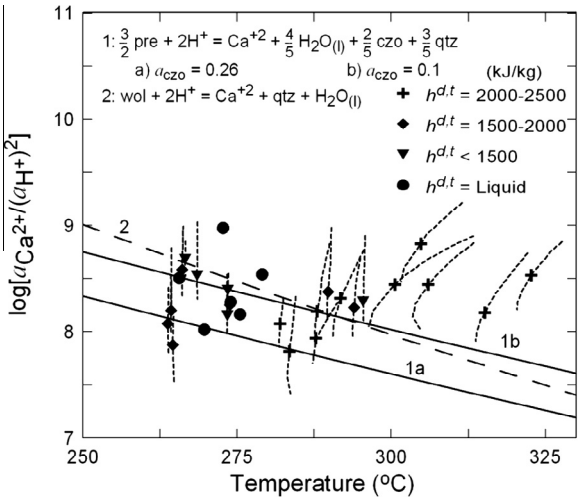

Fig. 10. The logarithm of the Ca^{2+}/H^+ activity ratio in initial aquifer fluids. Dotted lines show the total range of variability arising from the assumed phase segregation conditions, which were varied from directly below the initial aquifer fluid temperature to immediately above the wellhead temperature.

concentrations of the acidic gases (CO_2 and H_2S), which were described above to be highly sensitive to the assumed phase segregation conditions (Fig. 5). The increased departure from equilibrium at >290 °C may also indicate the maximum temperature limit of prehnite or reflect onset of control by a mineral assemblage including actinolite, which is formed at these temperatures (Kristmansdóttir, 1979). However, this margin of uncertainty does not change the general observation of a close approach to mineral–fluid equilibrium, in line with previous conclusions (Stefánsson and Arnórsson, 2000, 2002).

There are two main approaches to using gases to assess equilibrium in the reservoir. In the first one, liquid-phase activities of the volatile species are assumed to be controlled by equilibrium with respect to specific secondary mineral assemblages (Arnórsson et al., 1983, 2010; Stefánsson and Arnórsson, 2002; Karingithi et al., 2010). In the second one, gas concentrations are assumed to be fixed by redox reactions among vapor-phase components and the rock (Giggenbach, 1980, 1987; D'Amore et al., 1993). The equilibrium curves of the mineral assemblages that could potentially fix the activities of the main reactive gases CO_2, H_2S and H_2 (method 1) are compared with their calculated aquifer fluid compositions in Fig. 11a–c. A reasonably close comparison was observed for H_2S and H_2, assuming equilibrium with minerals including pyrite, pyrrhotite, prehnite, epidote and possibly also magnetite. The difference in equilibrium concentrations for the different possible mineral reactions is smaller than the uncertainty arising from the phase segregation model. Based on this, it is not possible to unambiguously conclude which mineral buffer is responsible for controlling H_2S and H_2. The calculated equilibrium vapor fractions assuming equilibrium with respect to the pyrite, pyrrhotite, prehnite, epidote mineral assemblage are shown in Fig. 12 for H_2. Most equilibrium vapor fractions are low and positive, giving a field average

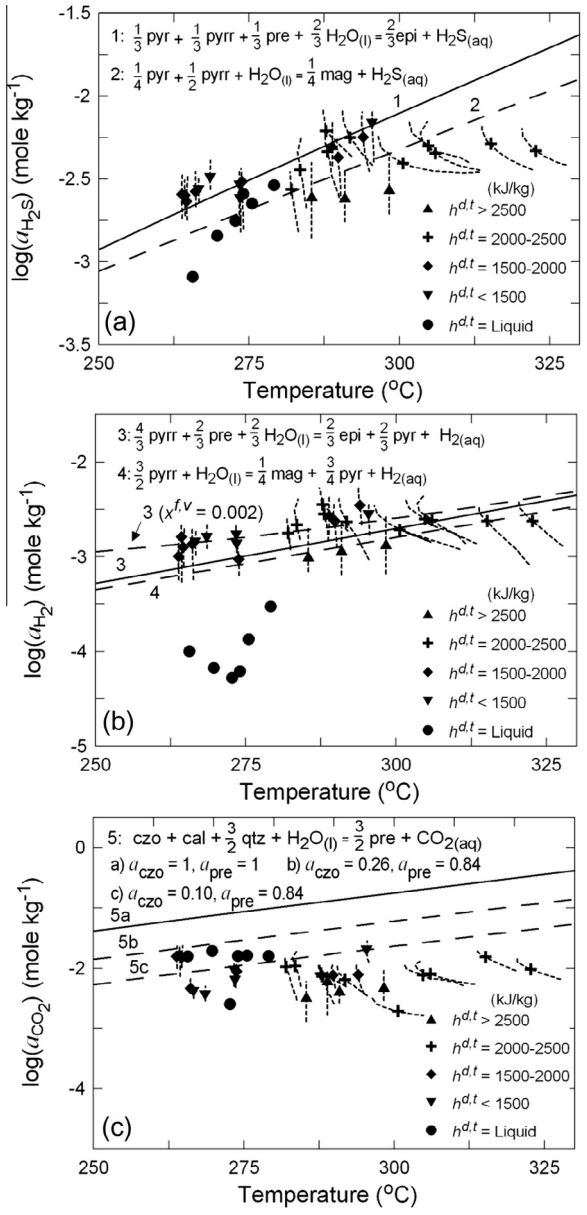

Fig. 11. Mineral buffer reaction equilibrium for H_2S, H_2 and CO_2. Dotted lines show the total range of variability due to assumed phase segregation conditions, which were varied from directly below the initial aquifer fluid temperature to immediately above the wellhead temperature.

of approximately 0.2% by mass. Several of the highest excess enthalpy wells show lower or even slightly negative equilibrium vapor fractions. These are believed to be erroneous, a consequence of the fact that conductive heat transfer contributes slightly to the excess enthalpy in these wells and ignoring this in model calculations results in underestimated aquifer fluid gas concentrations (Fig. 6). Alternatively, they could be related to errors in the selected aquifer fluid temperature or phase segregation pressure (Fig. 9).

Carbon dioxide concentrations are observed to be somewhat low in comparison to equilibrium values with respect

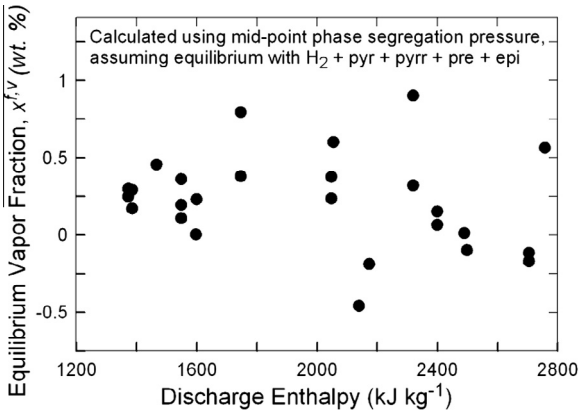

Fig. 12. Calculated equilibrium vapor fractions versus well discharge enthalpy, assuming equilibrium of H_2 with respect to the pyrite, pyrrhotite, prehnite and epidote mineral buffer.

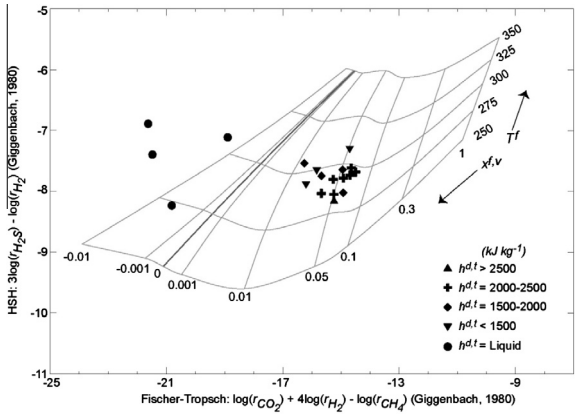

Fig. 13. FT-HSH plot for reservoir fluids according to the method of Giggenbach (1980). Total aquifer gas concentrations calculated using model 3, assuming 'mid-point' phase segregation pressure. Calculations use thermodynamic data and partition coefficients for the gaseous species according to Giggenbach (1980) and were implemented using the Gas_Analysis_v2-Powell-2010-StanfordGW spreadsheet (Powell and Cumming, 2010).

to clinozoisite, calcite, quartz and prehnite, as was previously concluded (Stefánsson et al., 2011). Additionally, this discrepancy cannot be explained based solely on the uncertainties in the reconstruction of aquifer fluid composition. Other previously considered mineral assemblages that could control aqueous CO_2 include grossular (Karingithi et al., 2010), which is not commonly observed at Hellisheidi. It is somewhat unlikely that the low CO_2 concentrations are related to boiling and subsequent precipitation of calcite (Simmons and Christenson, 1994), as the concentrations of CO_2 and Ca^{2+} differ by roughly an order of magnitude, and the CO_2 concentration will hardly be affected even if most of the Ca^{2+} in solution has been removed. Evidence that CO_2 concentrations may be source- rather than equilibrium-controlled has from field studies showing significant short- and long-term changes in concentrations in response to magmatic events (Ármansson et al., 1989; Gudmundsson and Arnórsson, 2002), as well as experiments performed on rhyolitic rocks demonstrating the non-reactivity of CO_2 at

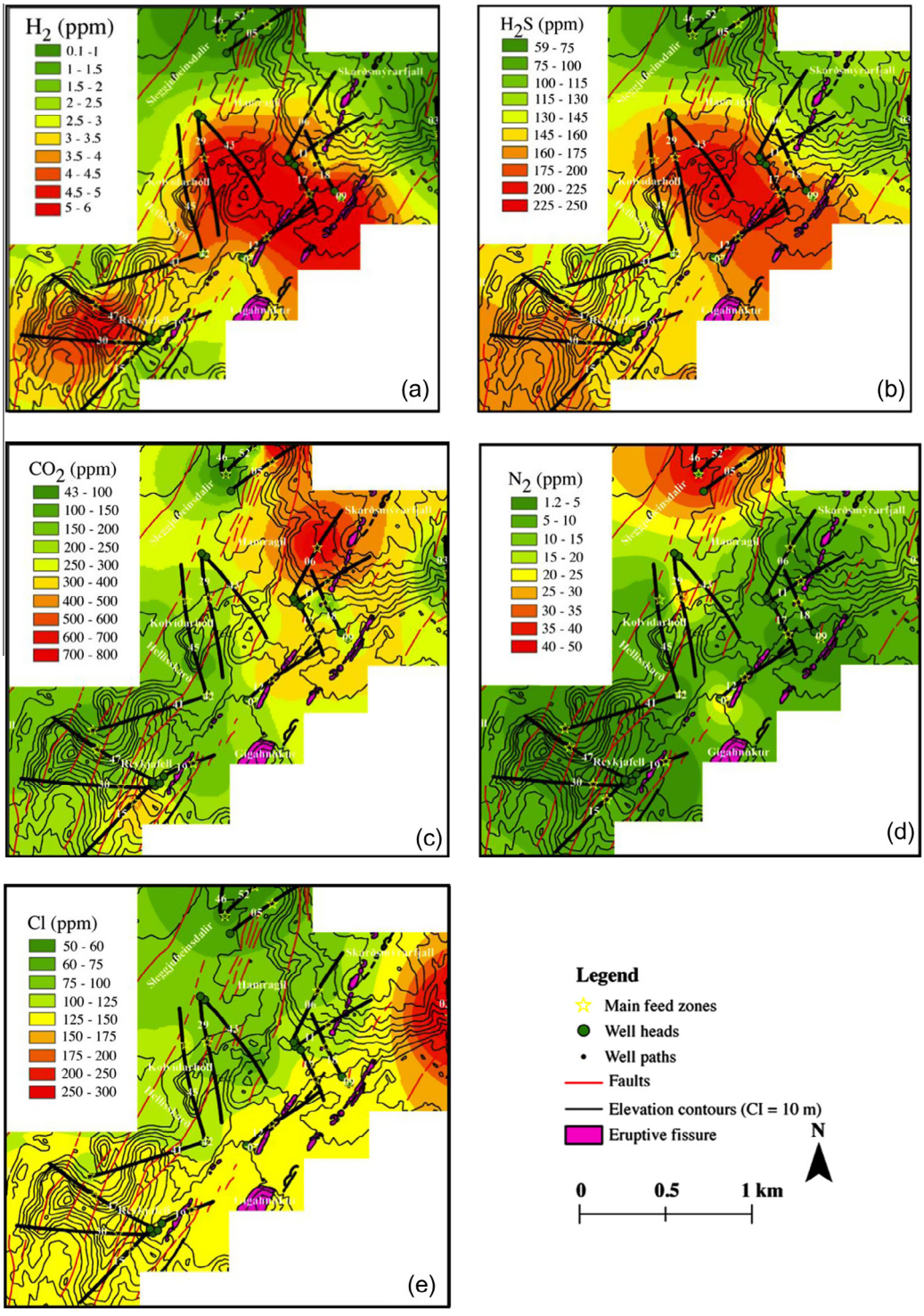

Fig. 14. Calculated distribution of (a) CO_2, (b) H_2S, (c) H_2, (d) N_2 and (e) Cl concentrations in aquifer fluids.

300 °C (Bischoff and Rosenbauer, 1996). This suggests that the low CO_2 concentrations may be source-controlled at Hellisheidi.

For estimation of aquifer vapor fraction based on gas concentrations (method 2), it is common to assume equilibrium for the Fischer–Tropsch reaction.

$$CH_4 + 2H_2O = 4H_2 + CO_2$$

as well as among H_2, H_2S and redox-sensitive minerals such as pyrite and magnetite according to a reaction such as:

$$FeS_2 + 2H_2 + 2H_2O = Fe_3O_4 + 6H_2S$$

Fig. 13 is a geothermometer and equilibrium vapor fraction grid based on equilibrium according to these reactions (FT-HSH plot). The results of aquifer temperatures are in good agreement with those derived from quartz geothermometry and the phase segregation model. On the other hand, the calculated equilibrium vapor fractions were approximately one order of magnitude higher. This discrepancy may simply be caused by redox disequilibrium among CH_4, H_2O, H_2 and CO_2 in line with previous studies on dilute geothermal fluids in Iceland (Stefánsson and Arnórsson, 2002). These results indicate that the application of gas concentrations to assessing reservoir conditions is not straightforward and relies on the assumption of redox equilibrium that simply may not prevail at temperatures <300 °C (Giggenbach, 1987; Stefánsson and Arnórsson, 2002).

8. CONCEPTUAL GEOCHEMICAL MODEL OF THE HELLISHEIDI GEOTHERMAL SYSTEM

Aquifer fluid compositions may be used to gain insight into the source and geochemistry of fluids in volcanic geothermal systems like Hellisheidi. When combined with other types of information derived from geology, borehole logging and hydrology, these may be used to make a conceptual model of the system. Information from fluid chemistry may be used to study for example fluid recharge, fluid up-flow and fluid–fluid and fluid–rock interaction. Some volatile and non-reactive elements may be of particular importance for such work, for example H_2, H_2S, CO_2, N_2 and Cl. Their distributions in the Hellisheidi geothermal field are shown in Fig. 14.

It was previously concluded that the aquifer concentrations of H_2S and H_2 are controlled by temperature-dependent equilibrium with secondary minerals. Accordingly, the highest concentrations of these gases should indicate the hottest parts of the system. However, some of the excess enthalpy wells drilled in the proximity of the eruptive fissure are somewhat lower in H_2 and H_2S (Fig. 14a and b). This is believed to be an artifact of the faulty assumption that the process of phase segregation produced all of the excess discharge enthalpy. While many of the wells sampled at Hellisheidi have relatively shallow feed zones (~1000 m depth) and slight temperature reversals, the wells in the proximity of the fissure have deeper feed zones (~2000 m) that discharge a fluid dominantly consisting of saturated steam. Conductive heat transfer from the rock to the fluid flowing into wells may well be more of a factor for these wells. In fact, when the effect of conductive heat transfer is taken into consideration for either H_2S and H_2, bringing up its calculated concentration enough to match the population described by the other excess enthalpy wells (either close to equilibrium for H_2S or slightly above equilibrium for H_2), the calculated concentration of the other gas increases sufficiently to match its population in these wells.

Carbon dioxide has a markedly different field-scale distribution than the equilibrium-controlled gases H_2S and H_2. The highest CO_2 concentrations are observed at the southern end of Skardsmýrarfjall below Hamragil

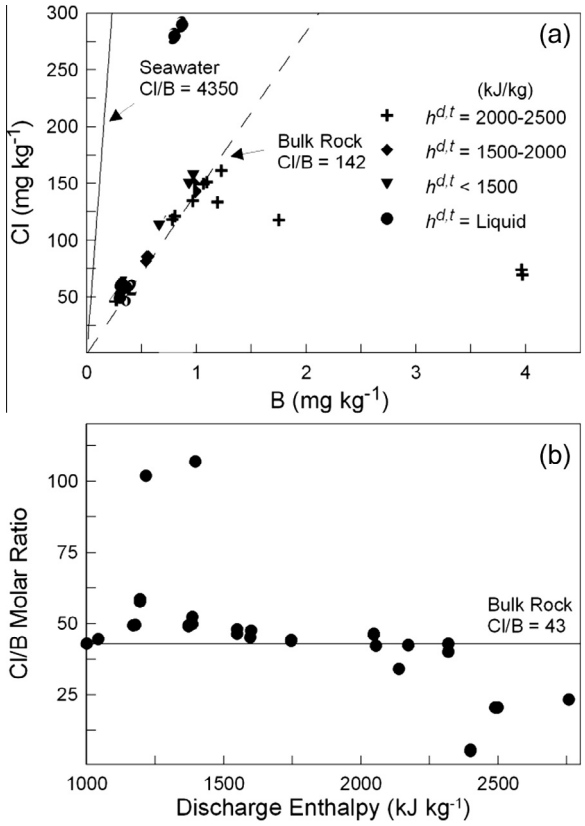

Fig. 15. (a) Cl/B mass ratio of aquifer fluids, compared with average ratio in tholeiitic basalt and seawater (Arnórsson and Andrésdóttir, 1995). (b) Cl/B molar ratio versus discharge enthalpy.

(Fig. 10c), outside of the hottest zone of the system according to down-hole temperature measurements (Gunnarsson et al., 2010) and H_2S and H_2 concentrations. Moreover, the present concentrations are not spatially related to the area of highest temperature and excess well discharge enthalpy near the eruptive fissure. If magmatic degassing is occurring to any substantial extent, the magma may be largely degassed with respect to CO_2 and unable to bring fluid concentrations up to equilibrium with the most likely mineral buffer (Fig. 11c). At the present moment, the exact controls on the CO_2 distribution in the Hellisheidi field are not well described.

The concentrations of N_2 and Cl are both considered to be mainly source-controlled and unaffected by secondary processes except boiling, with N_2 preferentially entering the steam phase and Cl retained in the liquid phase. The source of N_2 is considered to be the recharging air-saturated meteoric water whereas Cl originates from progressive fluid–rock interaction, seawater, or magma degassing. Except for a few wells, aquifer fluid N_2 concentrations are far below that of air-saturated water (Fig. 14d). Once recharging liquid is heated up close to the boiling point during the process of descent along the vertical fractures that serve as the main recharge channels for the reservoir, N_2 will strongly partition into the small fraction of steam that has been generated. Boiling geothermal systems can be

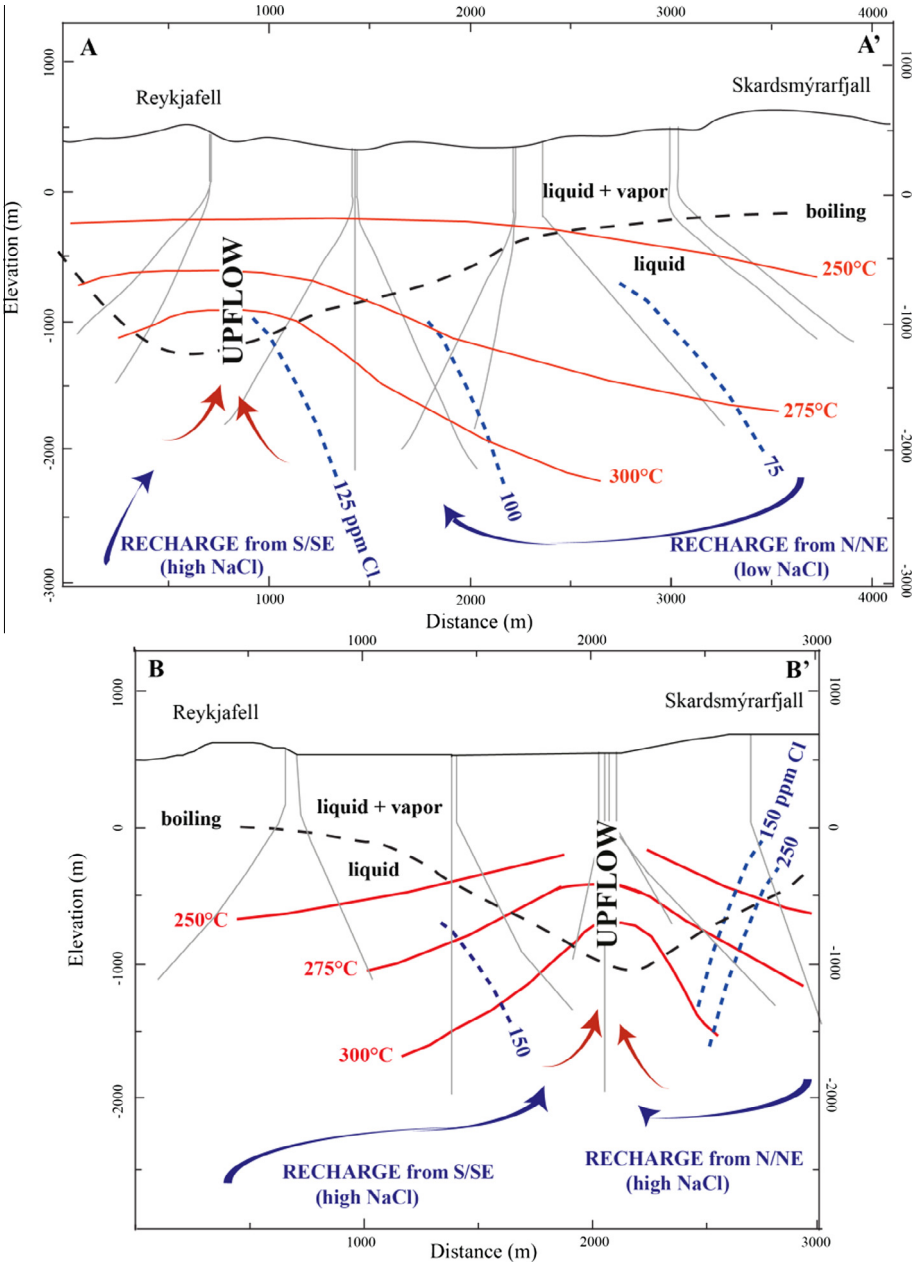

Fig. 16. A conceptual geochemical model of the Hellisheidi geothermal system showing the two approximately NE–SW oriented cross-sections shown in Fig. 1(A–A′, along the W margin of the field, and B–B′, along the E margin). Isotherms calculated using quartz temperatures and measured depths of principal aquifers. The extent of boiling is denoted by the black dashed line. The blue dashed lines show approximate Cl contours. (For interpretation of the references to color in this figure legend, the reader is referred to the web version of this article.)

expected to undergo this type of degassing nearly continuously, which could produce anomalously high concentrations of N_2 in shallower aquifers into which this steam rises. Although the cause of the very high N_2 concentrations in a few samples to the northwest of the field is not known and could indicate slight air contamination, in light of the low Cl concentrations present in this area, this area could also be a zone of inflow of more dilute (meteoric) waters.

Recharging meteoric waters are expected to have low Cl that increases with progressive fluid–rock interaction. In addition, seawater–meteoric water mixing may affect Cl concentration. There appears to be a mixing trend from the north to south, with Cl progressively increasing to the south (Fig. 14e). The Cl/B ratio (Fig. 15a) of most fluids falls on the bulk rock dissolution line, but the high Cl/B ratio of one sample suggests a slight seawater component in one well discharge close to the Hveragerdi geothermal area to the east, which is known to have a significant 'fossil' seawater component (Arnórsson and Andrésdóttir, 1995). Alternatively, the high Cl/B ratio in this discharge may be the consequence of late stage degassing of magma, as the

low solubility of boron in magma causes it to be lost from the magma at an early stage of degassing relative to Cl causing an increase in the Cl/B fluid ratio as degassing progresses.

A conceptual model of the geothermal system was developed based on regions of likely upflow, boiling and recharge (Fig. 16). There appear to be two distinct upflow zones – one on the western margin of the graben underlying Reykjafell and a smaller, shallower one on the eastern margin of the graben. Aside for the evidence presented above for locating the upflow zones here, including higher temperatures and enthalpies and deeper feedzones, the low Cl/B ratios observed in some of the wells in these areas (Fig. 15b) suggests that aquifer fluids have mixed with a deeper, hotter, dominantly vapor-like fluid enriched in B, which has a much stronger tendency than Cl to partition into the vapor phase at temperatures above 350 °C (Williams-Jones and Heinrich, 2005). Based on an initial aquifer fluid temperatures determined by quartz geothermometry, the measured depths of main producing aquifers (Gunnarsson et al., 2010), and the assumption of isenthalpic vertical upflow of saturated liquid until intersection of the boiling curve, liquid/vapor coexistence begins approximately 1.5 km b.s.l. and is suppressed on the margins of the upflows due to mixing with recharging waters at depth as well as lower heat input. Recent wells drilled into the southern part of the field have high temperatures (>300 °C) and discharge high excess enthalpy fluids (>2000 kJ/kg), suggesting that boiling may extend into this region.

9. SUMMARY AND CONCLUSIONS

Geothermal wells drilled into boiling aquifers commonly show excess enthalpy, where the enthalpy of the discharge is substantially higher than the enthalpy of vapor-saturated liquid at the aquifer temperature. A number of possible physical processes could account for this phenomenon, including conductive heat transfer from the aquifer rock to the flowing fluid, as well as loss or gain of liquid or vapor. In the case of the former, component concentrations are conserved and reconstruction of aquifer fluid composition is relatively straightforward. However, in the case of the latter, component concentrations are not conserved. In this study, aquifer compositions were modeled based on the assumption that the excess enthalpy of well discharges was completely due to the process of phase segregation, in which some fraction of the liquid flowing through the aquifer into the wellbore is retained in the rock formation. In addition to the aquifer fluid temperature, the main selected parameter is the temperature/pressure at which phase segregation is assumed to occur. This has been found to greatly impact the calculated concentration of volatiles in the aquifer fluid. However, since an initially vapor-saturated liquid attains a volumetric saturation corresponding to physical immobility approximately mid-way between the aquifer and well-head condition, an assumed phase segregation temperature/pressure conforming to this point is considered to be reasonable.

Even when taking into account the uncertainty due to the model calculations, this study confirms the general observation found of previous studies of a close approach to local fluid–mineral equilibria. Elevated H_2S and especially H_2 concentrations suggest the presence of an equilibrium vapor fraction in the aquifer fluid, indicative of boiling. However, CO_2 concentrations are lower than predicted by such equilibria, suggesting that other processes including magmatic degassing may be controlling. A conceptual model of the geothermal system has been proposed that stands in contrast to previous conceptual models of the field which predicted a central upflow zone above a magmatic heat source underlying the Hengill central volcano (e.g. Bödvarsson et al., 1990). While future studies should seek to further develop this conceptual model by considering isotopic data which was not available for this study, however this will also require determining the effect of phase segregation on the isotopic composition of produced fluids. Physiochemical aspects of boiling and phase segregation, including the pressure/temperature conditions at which it occurs or whether it results in significant mineral supersaturation and precipitation (e.g. sulfides, calcite) need to be better constrained. Additionally, while the permeability structure of the reservoir (i.e. pore- vs. fracture-bound) may also control the conditions of phase segregation, this role is not well understood. Furthermore, the exact nature of the magmatic heat source and the degree of interaction between it and aquifer fluids remain uncertain.

ACKNOWLEDGEMENTS

Reykjavik Energy is gratefully acknowledged for their financial support. Iceland Geosurvey (ÍSOR) is acknowledged for their support with geospatial data and temperature and pressure logs. We would also like to thank S. Hurwitz and two anonymous reviewers whose helpful comments led to significant improvements.

APPENDIX 1. MODELING OF AQUIFER FLUID COMPOSITION

List. of symbols

The symbology of Arnórsson et al. (2007) is adopted. Under this system, the first superscript indicates the location, or point, between the aquifer and discharge considered in the model. Thus, *f* refers to the feed zone beyond the zone of depressurization (initial aquifer fluid) and *d* to the discharge at the wellhead. Additionally, in the open system boiling model considered, *e* represents the intermediate zone of evaporation (depressurization zone) wherein liquid is retained by the aquifer or vapor added. The second superscript denotes the fluid phase(s) considered – *l* representing liquid, *v* vapor, and *t* the total two-phase fluid mixture. An extensive property specifically related to liquid retained in the formation is denoted by *lr* and for vapor added *va*. The subscript refers to the species or components considered – *s* to gaseous components, *r* to non-volatile components and *i* to either. A complete list of symbols is provided below.

ξ Degassing factor, with unity representing equilibrium degassing

ρ^l Density of saturated liquid at specified temperature/pressure (kg m^3)

ρ^v Density of saturated vapor at specified temperature/pressure (kg m^3)

D_s^e Distribution coefficient for volatile species s at the point of phase segregation

D_s^f Distribution coefficient for volatile species s in initial aquifer fluid

$h^{d,l}$ Enthalpy of saturated liquid at sampling pressure P^s (kJ kg^{-1})

$h^{d,t}$ Total enthalpy of well discharge (kJ kg^{-1})

$h^{d,v}$ Enthalpy of saturated vapor at sampling pressure P^s (kJ kg^{-1})

$h^{e,1}$ Enthalpy of saturated liquid at the point of phase segregation P^e (kJ kg^{-1})

$h^{e,v}$ Enthalpy of saturated vapor at phase segregation pressure P^e (kJ kg^{-1})

$h^{f,1}$ Enthalpy of saturated liquid at initial aquifer fluid conditions (kJ kg^{-1})

$h^{f,t}$ Total enthalpy of initial aquifer fluid. If $X^{f,v}$ is assumed to be 0, $h^{f,t} = h^{f,l}$ (kJ kg^{-1})

$h^{f,v}$ Enthalpy of saturated vapor at initial aquifer fluid conditions (kJ kg^{-1})

$h^{g,t}$ Total enthalpy of two-phase fluid immediately after phase segregation (kJ kg^{-1})

$K_{H,s}$ Henry's Law solubility constant for volatile species s

$m_i^{d,i}$ Concentration of chemical component i in liquid phase at sampling pressure P^s (moles kg^{-1})

$m_i^{d,t}$ Concentration of chemical component i in total well discharge (moles kg^{-1})

$m_i^{d,v}$ Concentration of chemical component i in vapor phase at sampling pressure P^s (moles kg^{-1})

$m_i^{e,l}$ Concentration of chemical component i in liquid phase at phase segregation pressure P^e (moles kg^{-1})

$m_i^{e,t}$ Concentration of chemical component i in total fluid immediately before phase segregation (moles kg^{-1})

$m_i^{e,v}$ Concentration of chemical component i in vapor phase at phase segregation pressure P^s (moles kg^{-1})

$m_i^{f,l}$ Concentration of chemical component i in liquid phase of initial aquifer fluid (moles kg^{-1})

$m_i^{f,t}$ Concentration of chemical component i in initial aquifer fluid (moles kg^{-1})

$m_r^{d,l}$ Concentration of non-volatile r in liquid phase at sampling pressure P^s (moles kg^{-1})

$m_r^{d,t}$ Concentration of non-volatile r in total well discharge (moles kg^{-1})

$m_r^{e,l}$ Concentration of non-volatile r in liquid phase at phase segregation pressure P^s (moles kg^{-1})

$m_r^{e,t}$ Concentration of non-volatile r in total fluid immediately prior to phase segregation (moles kg^{-1})

$m_r^{e,v}$ Concentration of non-volatile r in vapor phase at phase segregation pressure P^e (moles kg^{-1})

m_r^f, l Concentration of non-volatile r in liquid phase of initial aquifer fluid (moles kg^{-1})

$m_r^{f,t}$ Concentration of non-volatile r in total initial aquifer fluid (moles kg^{-1})

$m_r^{f,t,mid}$ Concentration of non-volatile r in total initial aquifer fluid calculated using mid-point phase segregation pressure $P^{e,mid}$ (moles kg^{-1})

$m_s^{d,l}$ Concentration of volatile species s in liquid phase at sampling pressure P^s (moles kg^{-1})

$m_s^{d,t}$ Concentration of volatile species s in total well discharge (moles kg^{-1})

$m_s^{d,v}$ Concentration of volatile species s in vapor phase at sampling pressure P^s (moles kg^{-1})

$m_s^{e,l}$ Concentration of volatile species s in liquid phase at phase segregation pressure P^e (moles kg^{-1})

$m_S^{e,t}$ Concentration of volatile species s in total fluid immediately prior to phase segregation (moles kg^{-1})

$m_s^{e,v}$ Concentration of volatile species s in vapor phase at phase segregation pressure P^e (moles kg^{-1})

$m_s^{f,t}$ Concentration of volatile species s in in total aquifer fluid (moles kg^{-1})

$m_s^{f,t,mid}$ Concentration of non-volatile r in total initial aquifer fluid calculated using mid-point phase segregation pressure $P^{e,mid}$ (moles kg^{-1})

$m_s^{f,l}$ Concentration of volatile species s in in aquifer liquid (moles kg^{-1})

$m_s^{f,v}$ Concentration of volatile species s in in aquifer vapor (moles kg^{-1})

$M^{d,l}$ Mass flow of liquid in well discharge (kg s^{-1})

$M^{d,t}$ Mass flow of liquid and steam in wet-steam well discharge (kg s^{-1})

$M^{d,v}$ Mass flow of steam in well discharge (kg s^{-1})

$M^{e,lr}$ Mass flow of boiled aquifer liquid which separates from steam flowing into well (kg s^{-1})

$M^{e,va}$ Mass flow of vapor added into two-phase flow flowing into well, following phase segregation (kg s^{-1})

$M^{f,t}$ Mass flow of total initial aquifer fluid into well (kg s^{-1})

P^e Vapor pressure at which phase segregation is assumed to occur (bar-a)

$P^{e,\mathrm{mid}}$ 'Mid-point' phase segregation pressure approximately halfway between P^f and P^{Wh} (bar-a)

P^f Saturation pressure at initial aquifer fluid temperature T^f (bar-a)

P^{wh} Vapor pressure as read from gauge attached to well-head (bar-g)

p^s Vapor pressure as read from gauge atop Webre separator (bar-g)

p_{sat} Vapor saturation pressure at a given temperature (bar-a)

p_{tot} Total fluid pressure, i.e. vapor pressure plus the partial pressures of all gases (bar-a)

Q^e Magnitude of conductive heat transfer from the rock formation to flowing two-phase fluid (kJ)

r_s Molar gas/water ratio of volatile species s in vapor phase ($m_s/m_{\mathrm{H_2O}}$) (–)

S^l Liquid volumetric saturation, with 0 representing pure vapor and 1 pure liquid (–)

T^e Saturation temperature at phase segregation pressure p^e (°C)

$T^{e,mid}$ Saturation temperature at the 'mid-point' phase segregation pressure $p^{e,mid}$ (°C)

$T_{\mathrm{qtz}}{}^f$ Temperature of initial aquifer fluid calculated according to quartz geothermometer of Gunnarsson and Arnórsson (2000) and using the mid-point phase segregation pressure (°C)

$T_{\mathrm{Na/K}}{}^f$ Temperature of initial aquifer fluid calculated according to Na/K geothermometer of Arnórsson and Stefánsson (1999) (°C)

T^f Selected temperature of initial aquifer fluid (°C)

$X^{d,v}$ Mass fraction of vapor at sampling pressure p^s

$X^{e,v}$ Mass fraction of vapor immediately prior to phase segregation

$X^{f,v}$ Vapor mass fraction present in the initial aquifer fluid (see Appendix 2, Equilibrium vapor fraction)

$\mathrm{V}^{\mathrm{e},lr}$ Relative mass of boiled water retained in aquifer upon phase segregation to well discharge ($M^{e,lr}/M^{d,t}$)

$V^{e,va}$ Relative mass of vapor added to flow following phase segregation to well discharge ($M^{e,va}/M^{d,t}$)

$V^{f,t}$ Relative mass of total inflowing initial aquifer fluid to well discharge ($M^{f,lr}/M^{d,t}$) For model 3, $V^{f,t} = (h^{d,t} - h^{e,l})/(h^{f,t} - h^{e,l})$ but for models 4 and 5 it is calculated slightly differently (see notes in Tables A.1 and A.2)

$Z^{e,v}$ Mass fraction of vapor immediately prior to phase segregation, including the effects of conductive heat transfer to the flowing two-phase fluid before phase segregation in model 5.

Aquifer. fluid composition

The models considered have been previously described in detail by Arnórsson et al. (2007, 2010). In model 1, isolated system boiling is assumed. In model 2, closed system boiling (conductive heat flow) is assumed. However, in models 3–5 open system boiling is assumed with possible transfer of heat and mass. Model 3 assumes no heat transfer upon boiling and that liquid water is partially retained in the aquifer but all the vapor flows into wells, whereas models 4 and 5 allow for vapor addition and conductive heat transfer in addition to phase segregation, respectively. Model 6 assumes loss of steam. The conservation equations for mass, enthalpy and mole numbers of non-volatile and volatile components are shown in Table A.1.

The equations to calculate non-volatile component concentrations in the initial aquifer based on measured concentrations in discharge fluids have been derived in Arnórsson et al. (2007, 2010). These are shown in Table A.2.

For volatile components, reconstructing aquifer fluid compositions from surface measurements requires the assumption of equilibrium distribution of the volatile species between the two phases at both the point of phase

Table A.1. Conservation equations for mass, enthalpy and mole numbers of non-volatile and volatile components.

Model	Mass flow equation	Specific enthalpy equation
1	$M^{d,t} = M^{f,t}$	$h^{d,t} \cdot M^{d,t} = h^{f,t} \cdot M^{f,t}$
2	$M^{d,t} = M^{f,t}$	$h^{d,t} \cdot M^{d,t} = h^{f,t} \cdot M^{f,t} + Q^{e}$
3	$M^{d,t} = M^{f,t} - M^{e,l}$	$h^{d,t} \cdot M^{d,t} = h^{f,t} \cdot M^{f,t} - h^{e,l} \cdot M^{e,l}$
4	$M^{d,t} = M^{f,t} - M^{e,l} + M^{e,va}$	$h^{d,t} \cdot M^{d,t} = h^{f,t} \cdot M^{f,t} - h^{e,l} \cdot M^{e,l} + h^{e,v} \cdot M^{e,va}$
5	$M^{d,t} = M^{f,t}$ - $M^{e,l}$	$h^{d,t} \cdot M^{d,t} = h^{f,t} \cdot M^{f,t} - h^{e,l} \cdot M^{e,l} + Q^{e}$
6	$M^{d,t} = M^{f,t}$ - $M^{e,v}$	$h^{d,t} \cdot M^{d,t} = h^{f,t} \cdot M^{f,t} - h^{e,v} \cdot M^{e,v}$
	Non-volatile component	Volatile component
1 and 2	$m_r^{d,t} \cdot M^{d,t} = m_r^{f,t} \cdot M^{f,t}$	$m_s^{d,t} \cdot M^{d,t} = m_s^{f,t} \cdot M^{f,t}$
3–5[a]	$m_r^{d,t} \cdot M^{d,t} = m_r^{f,t} \cdot M^{f,t} - m_r^{e,l} \cdot M^{e,l}$	$m_s^{d,t} \cdot M^{d,t} = m_s^{f,t} \cdot M^{f,t} - m_s^{e,l} \cdot M^{e,l}$
6	$m_r^{d,t} M^{d,t} = m_r^{f,t} \cdot M^{f,t}$	$m_r^{d,t} \cdot M^{d,t} = m_r^{f,t} \cdot M_{f,t} - m_r^{e,v} \cdot M_{e,v}$

[a]The concentration of chemical components in the added vapor in model 4 is assumed to be zero. As noted by Arnórsson et al. (2007), this is a poor approximation at the onset of boiling, but improves as production from the field progresses and the boiling fraction increases.

Table A.2. Equations to calculate non-volatile component concentrations in the initial aquifer based on measured concentrations in discharge fluids.

Model	Volatile species, aquifer liquid
1 and 2	$m_s^{f,l} = m_s^{d,t}/(1 - X^{f,v})$
3	$m_r^{f,l} = [m_r^{d,t}/(1 - X^{f,v})][(1 - (1/(1 - X^{e,v}))) + (1/(1 - X^{e,v}))]^{-1}$
4[a]	$m_r^{f,l} = [m_r^{d,t}/(1 - X^{f,v})][V^{f,t}(1 - (1/(1 - X^{e,v}))) + (1/(1 - X^{e,v})) - V^{e,va}(1/(1 - X^{e,v}))]^{-1}$
5[b]	$m_r^{f,l} = [m_r^{d,t}/(1 - X^{f,v})][V^{f,t}(1 - (1/(1 - Z^{e,v}))) + (1/(1 - Z^{e,v}))]^{-1}$
6	$m^{f,l} = [m_r^{d,t}][V^{f,t}(1 - X^{f,v})]^{-1}$

[a]In model 4 it is assumed that the vapor is added after retention of liquid and thus does not affect the vapor fraction at the point of phase segregation. Also, for model 4, $V^{f,t} = (h^{d,t} - h^{e,l} - V^{e,va}(h^{e,va} - h^{e,l}))/(h^{f,t} - h^{e,l})$.

[b]There are two versions of model 5. Under case A, liquid is first retained in the aquifer followed by conduction of heat from the formation to the flowing fluid. Under case B, conductive heat transfer from the rock to the flowing fluid precedes the retention of liquid in the formation. For case A use the equation given for models 3 to obtain $m_r^{f,l}$, but for case B use the reported equation for model 5. Additionally, for model 5, $V^{f,t} = (h^{d,t} - h^{e,l} - Q^{e}/M^{d,t})/(h^{f,t} - h^{e,l})$. The term $Z^{e,v}$ accounts for the portion of vapor at the point of phase segregation generated by conductive heat transfer to the flowing fluid and is given as $Z^{e,v} = (h^{f,t} + Q^{e}/M^{f,t} - h^{e,l})/(h^{e,v} - h^{e,l})$.

Table A.3. Equations to calculate non-volatile species concentrations in the initial aquifer based on measured concentrations in discharge fluids.

Model	Volatile species, aquifer liquid	Volatile species, aquifer vapor
1 and 2	$m_s^{f,l} = m_s^{d,t}[X^{f,v}(D_s^f - 1) + 1]^{-1}$	$m_s^{f,v} = m_s^{d,t}[X^{f,v}(1 - (1 - D_s^f)) + 1/D_s^f]^{-1}$
3	$m_s^{f,l} = m_s^{d,t}[V^{f,t}(1 - (1/(X^{e,v}(D_s^e - 1) + 1)))+ (1/X^{e,v}(D_s^e - 1) + 1))]^{-1}[X^{f,v}(D_s^f - 1) + 1]^{-1}$	$m_s^{f,v} = m_s^{d,t}[V^{f,t}(1 - (1/(X^{e,v}(D_s^e - 1) + 1))) + (1/X^{e,v}(D_s^e - 1) + 1))]^{-1}[X^{f,v}(1 - (1/D_s^f)) + (1/D_s^f)]^{-1}$
4[a]	$m_s^{f,l} = m_s^{d,t}[V^{f,t}(1 - (1/(X^{e,v}(D_s^e - 1) + 1))) + (1/X^{e,v}(D_s^e - 1) + 1)) + V^{e,va}(1/(X^{e,v}(D_e^s - 1) + 1))]^{-1}[X^{f,v}(D_s^f - 1) + 1]^{-1}$	$m_s^{f,v} = m_s^{d,t}[V^{f,t}(1 - (1/(X^{e,v}(D_s^e - 1) + 1))) + (1/X^{e,v}(D_s^e - 1) + 1)) + V^{e,va}(1/(X^{e,v}(D_e^s - 1) + 1))]^{-1}[X^{f,v}(1 - (1/D_s^f)) + (1/D_s^f)]^{-1}$
5[b]	$m_s^{f,l} = m_s^{d,t}[V^{f,t}(1 - (1/(Z^{e,v}(D_s^e - 1) + 1))) + (1/Z^{e,v}(D_s^e - 1) + 1))]^{-1}[X^{f,v}(D_s^f - 1) + 1]^{-1}$	$m_s^{f,v} = m_s^{d,t}[V^{f,t}(1 - (1/(Z^{e,v}(D_s^e - 1) + 1))) + (1/Z^{e,v}(D_s^e - 1) + 1))]^{-1}[X^{f,v}(1 - (1/D_s^f)) + (1/D_s^f)]^{-1}$
6[c]	$m_s^{f,l} = m_s^{d,t}[V^{f,t}(1 - X^{e,v})((1/D_s^e) - 1) + 1]^{-1}[X^{e,v}(1 - (1/D_s^e)) + (1/D_s^e)][X^{f,v}(D_s^f - 1) + 1]^{-1}$	$m_s^{f,l} = m_s^{d,t}[V^{f,t}(1 - X^{e,v})((1/D_s^e) - 1) + 1]^{-1}[X^{e,v}(1 - (1/D_s^e)) + (1/D_s^e)][X^{f,v}[X^{f,v}(1 - (1/D_s^f)) + (1/D_s^f)]^{-1}$

[a]See note [a] in Table A.1 above and note [a] in Table A.2 above.
[b] See note [b] in Table A.2 above.
[c]Alternatively, one can assume that $m_s^{f,l}$ is controlled by mineral-gas equilibria to obtain a value for $h^{f,t}$ by solving the system of equations iteratively (see Arnórsson et al., 2010).

segregation and within the initial aquifer fluid. The distribution coefficient D_s is a function of gas solubility and fluid pressure, defined $D_s = m_s^{f,v}/m_s^{f,l} = 55.508 \cdot \zeta/p_{tot} \cdot K_{H,s}$ where $K_{H,s}$ is the Henry's Law coefficient (moles kg^{-1} bar^{-1}) for a certain gas species s (these have been tabulated as a function of temperature in i.e. Arnórsson et al., 2007), p_{tot} the vapor pressure, p_{sat}, plus the sum of partial pressures of all gaseous components (since the partial pressures of non-condensable gas species contribute little relative to vapor pressure, $p_{tot} \approx p_{sat}$), ξ is a degassing factor (usually assumed to be unity, representing equilibrium degassing) and 55.508 is a factor for converting 1 kg of H_2O into moles of H_2O (see Arnórsson et al., 2007, for complete derivation). The equations to calculate volatile species concentrations in the initial aquifer based on measured concentrations in discharge fluids are shown in Table A.3.

APPENDIX 2. – EQUILIBRIUM VAPOR FRACTION

The primary advantage of mineral-gas equilibria to estimate the initial aquifer vapor fraction $X^{f,v}$ is that chemical equilibrium between hydrothermal mineral assemblages and reactive gas concentrations in the aquifer liquid is generally closely approached (Fig. 11). The gas species typically used for equilibrium vapor calculations are H_2 and H_2S, since CO_2 is often source rather than equilibrium controlled. Both H_2 and H_2S partition into the vapor phase, as determined by their respective Henry's law constants and the total fluid pressure. Thus, if initial aquifer fluid concentrations of these gases, particularly H_2, are calculated to be in excess of equilibrium, this can be attributed to the presence of a vapor phase. The vapor fraction calculated in this way can be derived from a basic equation that relates the total aquifer fluid concentration of a gas species with its concentration in the liquid phase:

$$m_s^{f,t} = m_s^{f,l}[X^{f,v}(D_s^f - 1) + 1] = m_s^{f,l}[((h^{f,t} - h^{f,l})/(h^{f,v} - h^{f,l}))(D_s^f - 1) + 1] \quad (A.1)$$

In the above equation, $h^{f,l}$, $h^{f,v}$ and D_s^f can be determined by selecting the initial aquifer temperature and $m_s^{f,l}$ represents the equilibrium concentration of the gas species ($H_2°$ or $H_2S°$) for the selected fluid-mineral buffer (see e.g. Arnórsson et al., 2007, 2010). Additionally, $m_s^{f,t}$ can be calculated according to the selected model shown in Table A.3 by removing the last term in brackets in each equation (which accounts for partitioning between the liquid and vapor phases). For example, for model 3:

$$m_s^{f,t} = m_s^{d,t}[V^{f,t}(1 - (1/X^{e,v}(D_s^e - 1) + 1))) + (1/(X^{e,v}(D_s^e - 1) + 1))]^{-1} \quad (A.2)$$

$$m_s^{f,t} = m_s^{d,t}[V^{f,t}(1 - (1/(((h^{f,t} - h^{e,l})/(h^{e,v} - h^{e,l}))(D_s^e - 1) + 1))) + (1/(((h^{f,t} - h^{e,l})/(h^{e,v} - h^{e,l}))(D_s^e - 1) + 1)))]^{-1}$$

Once an aquifer fluid temperature has been selected as well as a phase segregation temperature/pressure, all variables in equation A.2 are known except for $h^{f,t}$. The $h^{f,t}$ value that provides the same $m_s^{f,t}$ in both equations A.1 and A.2 can be determined by an iterative process. When $m_s^{f,t}$ has been obtained so has $h^{f,t}$, allowing $X^{f,v}$ to be obtained. Alternatively, it is possible to obtain a value for p^e by finding a common solution for both gases (Arnórsson et al., 2007, 2010). This method is, however, not considered to be as reliable as is the selection of p^e and solving by the method outlined above.

REFERENCES

Arellano V. M., Torres M. A. and Barragán R. M. (2005) Thermodynamic evolution of the Los Azurfres, Mexico, geothermal reservoir from 1982 to 2002. *Geothermics* **34**, 592–616.

Árnason K., Eysteinsson H. and Hersir G. P. (2010) Joint 1D inversion of TEM and MT data and 3D inversion of MT data in the Hengill area, SW Iceland. *Geothermics* **39**, 13–34.

Ármansson H., Gíslason G. and Hauksson T. (1982) Magmatic gases in well fluids aid the mapping of flow pattern in a geothermal system. *Geochim. Cosmochim. Acta* **46**, 167–177.

Ármansson H., Benjamínsson J. and Jeffrey A. W. A. (1989) Gas changes in the Krafla geothermal system, Iceland. *Chem. Geol.* **76**, 175–196.

Arnórsson S. (1995) Geothermal systems in Iceland: Structure and conceptual models 1, High-temperature areas. *Geothermics* **24**, 561–602.

Arnórsson S. and Andrésdóttir A. (1995) Processes controlling the distribution of boron and chlorine in natural-waters in Iceland. *Geochim. Cosmochim. Acta* **59**, 4125–4146.

Arnórsson S. and Andrésdottir A. (1999) The dissociation constants of Al-hydroxy complexes at 0–350 °C and P_{sat}. In *Geochemistry of the Earth's Surface* (ed. H. Ármannsson). Balkema, Rotterdam, The Netherlands, pp. 425–428.

Arnórsson, S., Angcoy, E., Bjarnason, J. Ö., Giroud, N., Gunnarsson, I., Kaasalainen, H., Karingithi, C. W. and Stefánsson, A. (2010) Gas chemistry of volcanic geothermal systems. World Geothermal Congress. Bali, Indonesia. #1428 (abstr.).

Arnórsson S., Bjarnason J. Ö., Giroud N., Gunnarsson I. and Stefánsson A. (2006) Sampling and analysis of geothermal fluids. *Geofluids* **6**, 203–216.

Arnórsson S., Björnsson S., Muna Z. W. and Ojiambo S. B. (1990) The use of gas chemistry to evaluate boiling processes and initial steam fractions in geothermal reservoirs with an example from the Olkaria field, Kenya. *Geothermics* **19**, 497–514.

Arnórsson S., Gunnarsson I., Stefánsson A., Andrésdóttir A. and Sveinbjörnsdóttir Á. E. (2002) Major element chemistry of surface- and ground waters in basaltic terrain, N Iceland I. *Primary mineral saturation. Geochim. Cosmochim. Acta* **66**, 4015–4046.

Arnórsson S., Gunnlaugsson E. and Svavarsson H. (1983) The chemistry of geothermal waters in Iceland 2. Mineral equilibria and independent variables controlling water compositions. *Geochim. Cosmochim. Acta* **47**, 547–566.

Arnórsson S., Sigurdsson S. and Svavarsson H. (1982) The chemistry of geothermal waters in Iceland 1. Calculation of aqueous speciation from 0 °C to 370 °C. *Geochim. Cosmochim. Acta* **46**, 1513–1532.

Arnórsson S. and Stefánsson A. (1999) Assessment of feldspar solubility constants in water in the range 0 degrees to 350 C at vapor saturation pressures. *Am. J. Sci.* **299**, 173–209.

Arnórsson S., Stefánsson A. and Bjarnason J. Ö. (2007) Fluid–fluid interactions in geothermal systems. *Rev. Min. Geochem.* **65**, 259–312.

Bischoff J. L. and Rosenbauer R. J. (1996) The alteration of rhyolite in CO_2 charged water at 200 and 350 oC: The unreactivity of CO_2 at higher temperature. *Geochim. Cosmochim. Acta* **60**, 3859–3867.

Bjarnason, J. Ö. (2010) *The chemical speciation program WATCH, version 2.4*. ÍSOR – Iceland Geosurvey, Reykjavík, Iceland. Accessible at: <http://www.geothermal.is/software>.

Bödvarsson G. S., Björnsson S., Gunnarsson A., Gunnlaugsson E., Sigurdsson O., Stefánsson V. and Steingrímsson B. (1990) The Nesjavellir geothermal field, Iceland, Part 1. Field characteristics and development of a three-dimensional numerical model. *Geotherm. Sci. Tech.* **2**, 189–228.

Browne P. R. L. and Ellis A. J. (1970) The Ohaaki–Broadlands hydrothermal area, New Zealand: Mineralogy and related geochemistry. *Am. J. Sci.* **269**, 97–113.

Browne P. R. L. (1978) Hydrothermal alteration in active geothermal fields. *Ann. Rev. Earth Plant. Sci.* **6**, 229–250.

D'Amore F. and Celati R. (1983) Methodology for calculating steam quality in geothermal reservoirs. *Geothermics* **12**, 129–140.

D'Amore F. and Truesdell A. H. (1985) Calculation of geothermal reservoir temperatures and steam fractions from gas compositions. *Trans. Geotherm. Res. Council* **9**, 305–310.

D'Amore F., Ramos-Candelaria M., Seastres J. S., Ruaya J. and Nuti S. (1993) Applications of gas chemistry in evaluating physical processes in the Southern Negros (Palinpinon) geothermal field, Philippines. *Geothermics* **22**, 535–553.

Diakonov I. I., Schott J., Martin F., Harrichourry J. C. and Escalier J. (1999) Iron(III) solubility and speciation in aqueous solutions. Experimental study and modelling: Part 1. Hematite solubility from 60 to 300 degrees C in NaOH–NaCl solutions and thermodynamic properties of $Fe(OH)_4^-$ (aq). *Geochim. Cosmochim. Acta* **63**, 2247–2261.

Ellis A. J. and Mahon W. A. J. (1977) *Chemistry and geothermal systems*. Academic Press, New York.

Faust C. R. and Mercer J. W. (1979) Geothermal reservoir simulation 1. Mathematical models for liquid- and vapor-dominated hydrothermal systems. *Wat. Res. Res.* **15**, 23–30.

Fernandez-Prini R., Alvarez J. L. and Harvey A. H. (2003) Henry's constants and vapor–liquid distribution constants for gaseous solutes in H_2O and D_2O at high temperatures. *J. Phys. Chem. Ref. Data* **32**, 903–916.

Foulger G. R. (1995) The Hengill geothermal area, Iceland – Variation of temperature-gradients deduced from the maximum depth of seismogenesis. *J. Volcanol. Geoth. Res.* **65**, 119–133.

Fournier R. (1981) Application of water geochemistry to geothermal exploration and reservoir engineering. In *Geothermal Systems: Principles and Case Histories* (eds. L. Rybach and L. Muffler). Wiley, New York, pp. 109–143.

Giggenbach W. F. (1980) Geothermal gas equilibria. *Geochim. Cosmochim. Acta* **44**, 2021–2032.

Giggenbach W. F. (1981) Geothermal mineral equilibria. *Geochim. Cosmochim. Acta* **45**, 393–410.

Giggenbach W. F. (1987) Redox processes governing the chemistry of fumarolic gas discharges from White Island, New Zealand. *Appl. Geochem.* **2**, 143–161.

Giggenbach W. F. (1988) Geothermal solute equilibria – derivation of Na–K–Mg–Ca geoindicators. *Geochim. Cosmochim. Acta* **52**, 2749–2765.

Giggenbach W. F. (1992) Isotopic shifts in waters from geothermal and volcanic systems along convergent plate boundaries and their origin. *Earth Planet. Sci.* **113**, 495–510.

Grant M. A. and Bixley P. F. (2011) *Geothermal Reservoir Engineering – Second Edition*. Academic Press, Burlington, Vermont.

Gudmundsson B. Th. and Arnórsson S. (2002) Geochemical monitoring of the Krafla and Námafjall geothermal areas, N-Iceland. *Geothermics* **31**, 195–243.

Gudmundsson B. Th. and Arnórsson S. (2005) Secondary mineral–fluid equilibria in the Krafla and Námafjall geothermal systems, Iceland. *Appl. Geochem.* **20**, 1607–1625.

Gunnarsson I. and Arnórsson S. (2000) Amorphous silica solubility and the thermodynamic properties of H_4SiO_4 in the range of 0 to 350 °C at P-sat. *Geochim. Cosmochim. Acta* **64**, 2295–2307.

Gunnarsson G., Arnaldsson A. and Oddsdóttir A. L. (2010) Model simulations of the Hengill area, southwestern Iceland. *Transp. Porous Med.* **90**, 3–22.

Henley R. W. and Hughes G. O. (2000) Underground fumaroles: "Excess heat" effects in vein formation. *Econ. Geol.* **95**, 453–466.

Holland T. J. B. and Powell R. (1998) An internally consistent thermodynamic data set for phases of petrological interest. *J. Metamorph. Geol.* **16**, 309–343.

Horne, R.N., Satik, C., Mahiya, G., Li, K., Ambusso, W., Tovar, R., Wang, C. and Nassori, H. (2000) Steam–water relative permeability. World Geothermal Congress. Kyushu-Tohuku, Japan. #R0347 (abstr.).

Johnson J. W., Oelkers E. H. and Helgeson H. C. (1992) Supcrt92 – a software package for calculating the standard molal thermodynamic properties of minerals, gases, aqueous species, and reactions from 1 bar to 5000 bar and 0 °C to 1000 °C. *Comput. Geosci.* **18**, 899–947.

Karingithi C. W., Arnórsson S. and Grönvold K. (2010) Processes controlling aquifer fluid compositions in the Olkaria geothermal system, Kenya. *J. Volcanol. Geoth. Res.* **196**, 57–76.

Kieffer S. and Delaney J. (1979) Isentropic decompression of fluids from crustal and mantle pressures. *J. Geophys. Res.* **84**, 1611–1620.

Kristmansdóttir H. (1979) Alteration of Basaltic Rocks by Hydrothermal Activity at 100–300 °C. *Dev. Sedimentol.* **27**, 359–367.

Larsson D., Grönvold K., Óskarsson N. and Gunnlaugsson E. (2002) Hydrothermal alteration of plagioclase and growth of secondary feldspar in the Hengill volcanic centre, SW Iceland. *J. Volcanol. Geoth. Res.* **114**, 275–290.

Li K. and Horne R. N. (2007) Systematic study of steam–water capillary pressure. *Geothermics* **36**, 558–574.

Lu X. and Kieffer S. (2009) Thermodynamics and mass transport in multicomponent, multiphase H_2O systems of planetary interest. *Ann. Rev. Earth Plant. Sci.* **37**, 449–477.

Mutonga, M.W., Sveinbjornsdóttir, Á, Gislason, G., and Ármansson, H. (2010) The Isotopic and Chemical Characteristics of Geothermal Fluids in Hengill Area, SW Iceland. World Geothermal Congress. Bali, Indonesia. #1434 (abstr.).

Piquemal J. (1994) Saturated steam relative permeabilities of unconsolidated porous media. *Transp. Porous Med.* **17**, 105–120.

Plummer L. N. and Busenberg E. (1982) The solubilities of calcite, aragonite and vaterite in CO_2–H_2O solutions between 0 °C and 90 °C, and an evaluation of the aqueous model for the system $CaCO_3$–CO_2–H_2O. *Geochim. Cosmochim. Acta* **46**, 1011–1040.

Pokrovskii G. S., Schott J., Salvi S., Gout R. and Kubicki J. D. (1998) Structure and stability of aluminium–silica complexes in neutral to basic solution. Experimental study and molecular orbital calculations. *Min. Mag.* **62A**, 1194–1195.

Pokrovskii V. A. and Helgeson H. C. (1995) Thermodynamic properties of aqueous species and the solubilities of minerals at high pressures and temperatures: the system Al_2O_3–H_2O–NaCl. *Am. J. Sci.* **295**, 1255–1342.

Powell T. and Cumming W. (2010) Spreadsheets for geothermal water and gas geochemistry. Thirty-Fifth Workshop on Geothermal Reservoir Engineering. Stanford University, Stanford, California. SGP-TR-188 (abstr.).

Pritchett J. W. (2005) Dry-steam wellhead discharges from liquid-dominated geothermal reservoirs: a result of coupled nonequilibrium multiphase fluid and heat flow through fractured rock. In *Dynamics of Fluids and Transport in Fractured Rock* (eds. B. Faybishenko, P. A. Witherspoon and J. Gale). AGU, Washington, DC, pp. 175–181.

Pruess K. and Narasimhan T. N. (1982) On fluid reserves and the production of superheated steam from fractured, vapor-dominated geothermal reservoirs. *J. Geophys. Res.* **87**, 9329–9339.

Remoroza, A.I. (2010) Calcite mineral scaling potentials of high-temperature geothermal wells. M. Sc. thesis, Univ. of Iceland.

Robie R. A. and Hemingway B. S. (1995) Thermodynamic properties of minerals and related substances at 298.15 K and 1 bar (105 Pascals) pressure and at higher temperatures. *U.S. Geol. Survey Bull.* **2131**.

Sæmundsson K. (1967) Vulkanismus und Tektonik des Hengill – Gebietes in Sudwest-Island. *Acta Nat. Isl.* **2**, 109 pp..

Sæmundsson K. (1992) Geology of the Thingvallavatn area. *Oikos* **64**, 40–68.

Schiffman P. and Fridleifsson G. Ó. (1991) The smectite chlorite transition in drillhole NJ-15, Nesjavellir geothermal-field, Iceland – XRD, BSE and electron-microprobe investigations. *J. Metamorph. Geol.* **9**, 679–696.

Sinton J., Grönvold K. and Sæmundsson K. (2005) Postglacial eruptive history of the western volcanic zone, Iceland. *Geochem. Geophys. Geosyst.* **6**, 1–34.

Simmons S. F. and Christenson B. W. (1994) Origins of calcite in a boiling geothermal system. *Am. J. Sci.* **294**, 361–400.

Sorey M. L., Grant M. A. and Bradford E. (1980) Nonlinear effects in two-phase flow to wells in geothermal reservoirs. *Wat. Res. Res.* **16**, 767–777.

Stefánsson A. and Arnórsson S. (2000) Feldspar saturation state in natural waters. *Geochim. Cosmochim. Acta* **64**, 2567–2584.

Stefánsson A. and Arnórsson S. (2002) Gas pressures and redox reactions in geothermal fluids in Iceland. *Chem. Geol.* **190**, 251–271.

Stefánsson A., Gunnarsson I. and Giroud N. (2007) New methods for the direct determination of dissolved inorganic, organic and total carbon in natural waters by reagent-free (TM) ion chromatography and inductively coupled plasma atomic emission spectrometry. *Anal. Chim. Acta* **582**, 69–74.

Stefánsson A., Arnórsson S., Gunnarsson I., Kaasalainen H. and Gunnlaugsson E. (2011) The geochemistry and sequestration of H_2S into the hydrothermal system at Hellisheidi, Iceland. *J. Vol. Geoth. Res.* **202**, 179–188.

Sveinbjörnsdottir Á. E. and Johnsen S. J. (1992) Stable isotope study of the Thingvallavatn area. Groundwater origin, age and evaporation models. *Oikos* **64**, 136–150.

Tryggvason A., Rögnvaldsson S. T. and Flóvenz O. G. (2002) Three-dimensional imaging of the P- and S-wave velocity structure and earthquake locations beneath Southwest Iceland. *Geophys. J. Int.* **151**, 848–866.

Williams-Jones A. and Heinrich C. (2005) Vapor transport of metals and the formation of magmatic-hydrothermal ore deposits. *Econ. Geol.* **100**, 1287–1312.

Associate editor: Jun-ichiro Ishibashi